Journal of Computational and Applied Mathematics 393 (2021) 113539

Contents lists available at ScienceDirect

Journal of Computational and Applied Mathematics

journal homepage: www.elsevier.com/locate/cam

Analysis of a 2-field finite element solver for poroelasticity on quadrilateral meshes

Zhuoran Wang [a], Simon Tavener [b], Jiangguo Liu [b,*]

[a] *School of Mathematics (Zhuhai), Sun Yat-sen University, Zhuhai, Guangdong 519082, China*
[b] *Department of Mathematics, Colorado State University, Fort Collins, CO 80523-1874, USA*

ARTICLE INFO

Article history:
Received 8 August 2020
Received in revised form 23 February 2021

Keywords:
Arbogast–Correa spaces
Enriched Lagrangian finite elements
Poroelasticity
Quadrilateral meshes
Weak Galerkin

ABSTRACT

This paper presents a novel 2-field finite element solver for linear poroelasticity on convex quadrilateral meshes. The Darcy flow is discretized for fluid pressure by a lowest-order weak Galerkin (WG) finite element method, which establishes the discrete weak gradient and numerical velocity in the lowest-order Arbogast–Correa space. The linear elasticity is discretized for solid displacement by the enriched Lagrangian finite elements with a special treatment for the volumetric dilation. These two types of finite elements are coupled through the implicit Euler temporal discretization to solve poroelasticity problems. A rigorous error analysis is presented along with numerical tests to demonstrate the accuracy and locking-free property of this new solver.

1. Introduction

This paper concerns finite element methods for the Biot's model for linear poroelasticity on a bounded domain Ω during a time period $[0, T]$ as follows

$$\begin{cases} -\nabla \cdot (2\mu\varepsilon(\mathbf{u}) + \lambda(\nabla \cdot \mathbf{u})\mathbf{I}) + \alpha\nabla p = \mathbf{f}, \\ \partial_t\,(\alpha\nabla \cdot \mathbf{u} + c_0 p) + \nabla \cdot (-\mathbf{K}\nabla p) = s, \end{cases} \tag{1}$$

where $\mathbf{u}(\mathbf{x}, t)$ is the unknown solid displacement, $\varepsilon(\mathbf{u}) = \frac{1}{2}\left(\nabla\mathbf{u} + (\nabla\mathbf{u})^T\right)$ is the strain tensor, λ, μ are Lamé constants, $\sigma(\mathbf{u}) = 2\mu\varepsilon(\mathbf{u}) + \lambda(\nabla \cdot \mathbf{u})\mathbf{I}$ is the effective stress for the solid (here $\mathbf{I}$ is the identity matrix), $\mathbf{f}$ is a body force, $p(\mathbf{x}, t)$ is the unknown fluid pressure, $\mathbf{K}$ is the hydraulic conductivity tensor, s is the fluid source (here sink is treated as negative source), $c_0 \geq 0$ is the constrained storage capacity, and α (usually close to 1) is the Biot–Williams constant.

For the poroelasticity problem, we should consider the total stress

$$\widetilde{\sigma}(\mathbf{u}, p) = \sigma - p\mathbf{I}. \tag{2}$$

Dirichlet and Neumann boundary conditions are posed as

$$\mathbf{u}|_{\Gamma_D^{\mathcal{E}}} = \mathbf{u}_D, \qquad (\widetilde{\sigma}\mathbf{n})|_{\Gamma_N^{\mathcal{E}}} = \mathbf{t}_N, \tag{3}$$

and

$$p|_{\Gamma_D^{\mathcal{D}}} = p_D, \qquad (-\mathbf{K}\nabla p) \cdot \mathbf{n}|_{\Gamma_N^{\mathcal{D}}} = u_N, \tag{4}$$

* Corresponding author.
E-mail addresses: wangzhr25@mail.sysu.edu.cn (Z. Wang), tavener@math.colostate.edu (S. Tavener), liu@math.colostate.edu (J. Liu).

https://doi.org/10.1016/j.cam.2021.113539
0377-0427/

where $\mathbf{n}$ is the outward unit normal vector to $\partial\Omega$, which has a non-overlapping decomposition $\partial\Omega = \Gamma_D^{\mathcal{E}} \cup \Gamma_N^{\mathcal{E}}$ for solid and another non-overlapping decomposition $\partial\Omega = \Gamma_D^{\mathcal{D}} \cup \Gamma_N^{\mathcal{D}}$ for fluid. As for initial conditions, we have

$$p(\mathbf{x}, 0) = p_0, \qquad \mathbf{u}(\mathbf{x}, 0) = \mathbf{u}_0. \tag{5}$$

Usually, $\mathbf{u}_0 = \mathbf{0}$, which means that there is no deformation for the elastic medium at the beginning of the simulation.

Modeling poroelasticity is of great importance in a wide range of science and engineering disciplines such as cell biology, drug delivery, food processing, reservoir engineering, soil mechanics, and tissue engineering [1–4].

An early complete theory about poroelasticity was formulated in Biot's consolidation model [5]. A more recent rigorous mathematical analysis was presented in [6]. It is difficult to obtain analytical solutions for poroelasticity problems. Therefore, solving poroelasticity problems relies mainly on numerical methods.

Numerical methods for poroelasticity can be classified based on what variables are being solved.

- *2-field*: Solid displacement, fluid pressure; See [7–9];
- *3-field*: Solid displacement, fluid pressure and velocity; See [10–13];
- *4-field*: Solid displacement and stress, fluid pressure and velocity; See [14] for solvers that couple the Raviart–Thomas pair for velocity and pressure and the Arnold–Winther pair for stress and displacement.

A main challenge in numerical simulations of poroelasticity is the *poroelasticity locking* [13,15], which often appears as nonphysical pressure oscillations for low permeable or low compressible media. Although poroelasticity has been studied to some extent by the computational mathematics community [5,8,10–12,16–23], new applications like those in [2,4] raise new challenges that call for accessible efficient new numerical methods.

The simplicity of the 2-field approach is always attractive and hence pursued by this paper. The Darcy flow is discretized for fluid pressure by a lowest-order weak Galerkin finite element method, which establishes the discrete weak gradient and numerical velocity in the lowest-order Arbogast–Correa space [24]. The linear elasticity is discretized for solid displacement by the enriched Lagrangian finite elements with a special treatment for the volumetric dilation [7,25]. These two types of finite elements are coupled through the implicit Euler temporal discretization to solve poroelasticity problems on convex quadrilateral meshes. No stabilization is needed for this new solver. It has the least degrees of freedom, compared to other existing solvers.

The rest of this paper is organized as follows. Section 2 presents a WG finite element discretization for Darcy flow. Section 3 discusses discretization for linear elasticity based on the enriched Lagrangian finite elements. Section 4 develops a 2-field finite element solver based on the aforementioned two types of finite elements and the backward Euler temporal discretization. A complete rigorous analysis of this new solver is presented in Section 5. Section 6 presents numerical experiments to demonstrate the accuracy and locking-free property of this new solver. Section 7 concludes the paper with some remarks.

2. WG finite element discretization for Darcy flow

Compared to the continuous and discontinuous Galerkin methods, weak Galerkin finite element methods are relatively new but have some noticeable features. For the Darcy equation, WG methods can be established based on the primal formulation but possess local mass conservation and normal flux continuity [24,26,27]. WG methods use reconstructed discrete weak gradients in certain subspaces that have desired approximation properties. This approach produces a numerical Darcy velocity via post-processing based on a local L^2-projection. It avoids the hybridization procedure used in the classical mixed finite element methods. In this section, we briefly discuss the new WG method $(P_0, P_0; AC_0)$ for Darcy flow on quadrilateral meshes [24].

2.1. Arbogast-Correa spaces AC_0 on convex quadrilaterals

Compared to the classical Raviart–Thomas elements [28] or the Arnold–Boffi–Falk elements [29], the Arbogast–Correa elements constructed recently in [30] for convex quadrilaterals have better approximation properties and less degrees of freedom. The $AC_k (k \geq 0)$ spaces are constructed using both unmapped vector-valued polynomials and rational functions obtained via the Piola transformation.

Let E be a convex quadrilateral and $k \geq 0$ be an integer. The local Arbogast–Correa space on E is defined as

$$AC_k(E) = P_k^2(E) + \mathbf{x}\widetilde{P}_k(E) + \mathbb{S}_k(E), \tag{6}$$

where $P_k^2(E)$ is the space of bivariate vector-valued polynomials defined on E with total degree at most k, $\widetilde{P}_k(E)$ is the space of bivariate homogeneous scalar-valued polynomials with degree exactly k, and $\mathbb{S}_k(E)$ is a supplementary space of vector-valued rational functions obtained via the Piola transformation.

For convenience, we write $\mathbb{S}_k = \mathcal{P}_E\hat{\mathbb{S}}_k$, where $\mathcal{P}_E$ is the Piola transformation. Let $(\hat{x}, \hat{y})$ be the coordinates in the reference element $[0, 1]^2$. According to [30], for $k = 0$,

$$\hat{\mathbb{S}}_0 = \mathrm{span}\{\mathbf{curl}(\hat{x}\hat{y})\}. \tag{7}$$

For $k \geq 1$,

$$\hat{\mathbb{S}}_k = \text{span}\{\mathbf{curl}((1-\hat{x}^2)\hat{x}^{k-1}\hat{y}),\ \mathbf{curl}(\hat{x}^{k-1}\hat{y}(1-\hat{y}^2))\}. \tag{8}$$

Roughly speaking, $P_k^2(E)$ accounts for the approximation of a vector field on a convex quadrilateral, $\mathbf{x}\widetilde{P}_k(E)$ accounts for the approximation of divergence, and $\mathbb{S}_k$ offers a divergence-free supplement.

Given these discrete spaces, we have

$$\dim(P_k^2) = (k+1)(k+2), \qquad \dim(\widetilde{P}_k) = k+1,$$

and

$$\dim(\mathbb{S}_k) = 1 \ \text{ if } \ k=0, \qquad \dim(\mathbb{S}_k) = 2 \ \text{ if } \ k>0.$$

If we set $s_k = \dim(\mathbb{S}_k)$, then

$$\dim(AC_k(E)) = (k+1)(k+3) + s_k. \tag{9}$$

Note that $(k+1)(k+3) = \dim(RT_k)$, i.e., the dimension of the kth order Raviart–Thomas (RT) space on a triangle [28]. Thus, s_k represents the additional degrees of freedom needed for augmenting the RT space on a quadrilateral [30].

However, in this paper, only the lowest-order space AC_0 is used. More interestingly, a set of local basis functions for a general quadrilateral are

$$\begin{bmatrix}1\\0\end{bmatrix}, \quad \begin{bmatrix}0\\1\end{bmatrix}, \quad \begin{bmatrix}X\\Y\end{bmatrix}, \quad \mathcal{P}_E\begin{bmatrix}\hat{x}\\-\hat{y}\end{bmatrix}, \tag{10}$$

where $X = x - x_c$, $Y = y - y_c$ are the normalized coordinates with (x_c, y_c) being the element center, $(\hat{x}, \hat{y})$ are the reference coordinates in the reference element $[0,1]^2$, and $\mathcal{P}_E$ is the Piola transformation (matrix).

We need a local projection operator $\mathbf{Q}_h$ from $\mathbf{L}^2(E)$ to the space $AC_0(E)$ for any quadrilateral E. Given $\mathbf{v} \in \mathbf{L}^2(E)$, find $\mathbf{Q}_h\mathbf{v} \in AC_0(E)$ such that

$$(\mathbf{Q}_h\mathbf{v}, \mathbf{w})_E = (\mathbf{v}, \mathbf{w})_E, \qquad \forall \mathbf{w} \in AC_0(E). \tag{11}$$

Later on for error analysis in Section 5, we need also the global space $\mathcal{AC}_0(\mathcal{E}_h)$ on the whole mesh $\mathcal{E}_h$ and the global interpolation operator Π_h from $H(\text{div}, \Omega)$ to $\mathcal{AC}_0(\mathcal{E}_h)$.

2.2. $WG(P_0, P_0; AC_0)$ *finite elements for Darcy flow*

Weak Galerkin finite elements use separate basis functions in element interiors and on interelement boundaries. These basis functions are different than those used in the continuous or discontinuous Galerkin methods. We call them *discrete weak functions*.

Let $k \geq 0$ be an integer and E be a convex quadrilateral with interior E° and boundary E^∂. Let $P_k(E^\circ)$ be the space of polynomials defined in E° with degree at most k, and similarly, $P_k(E^\partial)$ be the space of piecewise polynomials defined on E^∂ with degree at most k. Let $AC_k(E)$ be the space of vector-valued functions discussed in the previous subsection.

Let $\phi = \{\phi^\circ, \phi^\partial\}$ be a discrete weak function such that $\phi^\circ \in P_k(E^\circ)$ and $\phi^\partial \in P_k(E^\partial)$. Note that ϕ° is defined for the element interior only; whereas ϕ^∂ is defined on the element boundary only. We define $\nabla_w\phi \in AC_k(E)$ by

$$\int_E (\nabla_w\phi)\cdot\mathbf{w} = \int_{E^\partial} \phi^\partial(\mathbf{w}\cdot\mathbf{n}) - \int_{E^\circ} \phi^\circ(\nabla\cdot\mathbf{w}), \qquad \forall \mathbf{w} \in AC_k(E), \tag{12}$$

or in slightly different notation

$$(\nabla_w\phi, \mathbf{w})_E = \langle \phi^\partial, \mathbf{w}\cdot\mathbf{n}\rangle_{E^\partial} - (\phi^\circ, \nabla\cdot\mathbf{w})_{E^\circ}. \tag{13}$$

This paper focuses on the case $k=0$. We deal with discrete weak functions that are constants separately defined in element interiors and on edges. In this case, equation (13) is simply a size-4 SPD linear system for each quadrilateral. Its solution contains 4 coefficients to be used for expressing $\nabla_w\phi$ as a linear combination of the local basis functions of AC_0 stated in (10).

We shall also need a local L^2-projection $Q_h = \{Q_h^\circ, Q_h^\partial\}$, where Q_h° is the L^2-projection that maps a function in $L^2(E^\circ)$ to a constant in E°, whereas Q_h^∂ is the L^2-projection that maps a function in $L^2(e)$ to a constant on e for each edge e on E^∂.

For convenience, we assume the Darcy flow is prototyped as

$$\begin{cases} \nabla\cdot(-\mathbf{K}\nabla p) \equiv \nabla\cdot\mathbf{u} = s, & \mathbf{x}\in\Omega, \\ p = p_D, & \mathbf{x}\in\Gamma_D^{\mathcal{D}}, \\ \mathbf{u}\cdot\mathbf{n} = u_N, & \mathbf{x}\in\Gamma_N^{\mathcal{D}}, \end{cases} \tag{14}$$

where Ω is a polygonal domain, p is the unknown fluid pressure, $\mathbf{K}$ a 2×2 hydraulic conductivity matrix that is uniformly symmetric positive-definite (SPD), s a known source, p_D, u_N Dirichlet and Neumann boundary data, respectively, $\mathbf{n}$ the outward unit normal vector to $\partial\Omega$ that has a nonoverlapping decomposition $\Gamma_D^{\mathcal{D}} \cup \Gamma_N^{\mathcal{D}}$.

WG scheme for pressure on a quadrilateral mesh. Assume $\mathcal{E}_h$ is a shape-regular convex quadrilateral mesh on Ω. Let S_h be the space of discrete weak shape functions that are constants in the element interiors and also constants on the edges in $\mathcal{E}_h$. Let S_h^0 be the subspace of S_h consisting of those shape functions that vanish on $\Gamma_D^{\mathcal{D}}$. Seek $p_h = \{p_h^\circ, p_h^\partial\} \in S_h$ such that $p_h^\partial|_{\Gamma_D^{\mathcal{D}}} = Q_h^\partial(p_D)$ and

$$\mathcal{A}_h(p_h, q) = \mathcal{F}_h(q), \qquad \forall q = \{q^\circ, q^\partial\} \in S_h^0, \tag{15}$$

where

$$\mathcal{A}_h(p_h, q) = \sum_{E\in\mathcal{E}_h} \int_E \mathbf{K}\nabla_w p_h \cdot \nabla_w q \tag{16}$$

and

$$\mathcal{F}_h(q) = \sum_{E\in\mathcal{E}_h} \int_{E^\circ} f\, q^\circ - \sum_{e\in\Gamma_N^{\mathcal{D}}} \int_e u_N q^\partial . \tag{17}$$

3. Linear elasticity discretization by enriched Lagrangian finite elements

In this section, we focus on discretization of linear elasticity, which is an important part of linear poroelasticity. We shall elaborate on the discretization on convex quadrilaterals based on the enriched Lagrangian finite elements [25].

Recall that linear elasticity on its own takes the following form

$$\begin{cases} -\nabla\cdot\sigma = \mathbf{f}(\mathbf{x}), & \mathbf{x}\in\Omega, \\ \mathbf{u}|_{\Gamma_D^{\mathcal{E}}} = \mathbf{u}_D, & (\sigma\mathbf{n})|_{\Gamma_N^{\mathcal{E}}} = \mathbf{t}_N, \end{cases} \tag{18}$$

where Ω is a two- or three-dimensional bounded domain occupied by a homogeneous and isotropic elastic body, $\mathbf{f}$ is a body force, $\mathbf{u}_D$, $\mathbf{t}_N$ are respectively boundary data about displacement and traction posed on the Dirichlet and Neumann boundaries $\Gamma_D^{\mathcal{E}}$ and $\Gamma_N^{\mathcal{E}}$, and $\mathbf{n}$ is the outward unit normal vector to the domain boundary $\partial\Omega$. As usual, $\mathbf{u}$ is the solid displacement, $\varepsilon(\mathbf{u}) = \frac{1}{2}\left(\nabla\mathbf{u} + (\nabla\mathbf{u})^T\right)$ is the strain tensor, and $\sigma = 2\mu\,\varepsilon(\mathbf{u}) + \lambda(\nabla\cdot\mathbf{u})\mathbf{I}$ is the Cauchy stress tensor, where $\mathbf{I}$ is the order-two or -three identity matrix. Note that the Lamé constants λ, μ are given by

$$\lambda = \frac{E\nu}{(1+\nu)(1-2\nu)}, \qquad \mu = \frac{E}{2(1+\nu)}, \tag{19}$$

where E is the Young's modulus and ν is Poisson's ratio.

A major challenge in development of numerical methods for linear elasticity is the *Poisson-locking*, which often appears as loss of convergence rates in displacement and/or suspicious behaviors in other quantities such as stress when $\lambda\to\infty$ or $\nu\to\frac{1}{2}$, namely, the material becomes nearly incompressible. It is well known that the linear Lagrangian elements Q_1^2 (for rectangles) or P_1^2 (for triangles) suffer Poisson-locking [15,31]. Remedies have been sought [32–35].

In this paper, we adopt the method developed in [25]. This method is actually a continuous Galerkin type method but free of Poisson-locking. It is realized by enriching the classical Q_1^2 Lagrangian elements by edge-based bubble functions.

Let E be a convex quadrilateral with vertices $P_i = (x_i, y_i)$, $i = 1,2,3,4$. Let e_i be the edge connecting P_{i-1} and P_i, $i = 1,2,3,4$. Of course, P_0 is understood as P_4, by the modulo convention. Let $\mathbf{n}_i$ be the outward unit normal vector on edge e_i, $i = 1,2,3,4$.

Let $\hat{E} = [0,1]^2$ (the unit square) be the reference element. Let $(\hat{x},\hat{y})$ be the reference variables. A bilinear mapping from $\hat{E}$ to E is established as

$$\begin{cases} x = a_1 + a_2\hat{x} + a_3\hat{y} + a_4\hat{x}\hat{y}, \\ y = b_1 + b_2\hat{x} + b_3\hat{y} + b_4\hat{x}\hat{y}, \end{cases} \tag{20}$$

where the eight coefficients $a_i, b_i (i = 1,2,3,4)$ can be directly calculated using the vertex coordinates:

$$\begin{aligned} &a_1 = x_1, \quad a_2 = x_2 - x_1, \quad a_3 = x_4 - x_1, \quad a_4 = (x_1+x_3) - (x_2+x_4), \\ &b_1 = y_1, \quad b_2 = y_2 - y_1, \quad b_3 = y_4 - y_1, \quad b_4 = (y_1+y_3) - (y_2+y_4). \end{aligned}$$

We first consider four scalar basis functions defined on $\hat{E}$:

$$\hat{\phi}_1(\hat{x},\hat{y}) = (1-\hat{x})(1-\hat{y}), \qquad \hat{\phi}_2(\hat{x},\hat{y}) = \hat{x}(1-\hat{y}), \tag{21}$$

$$\hat{\phi}_3(\hat{x},\hat{y}) = \hat{x}\hat{y}, \qquad \hat{\phi}_4(\hat{x},\hat{y}) = (1-\hat{x})\hat{y}. \tag{22}$$

Let $(x, y) \in E$ be the bilinear mapping image of $(\hat{x}, \hat{y}) \in \hat{E}$. We consider eight vector-valued Lagrangian $Q_1(E)^2$ basis functions on E:

$$\boldsymbol{\phi}_{2i-1}(x, y) = \begin{bmatrix} \hat{\phi}_i(\hat{x}, \hat{y}) \\ 0 \end{bmatrix}, \quad \boldsymbol{\phi}_{2i}(x, y) = \begin{bmatrix} 0 \\ \hat{\phi}_i(\hat{x}, \hat{y}) \end{bmatrix}, \quad i = 1, 2, 3, 4. \tag{23}$$

Now we consider four more scalar basis functions defined on $\hat{E}$:

$$\begin{aligned} \hat{\psi}_1(\hat{x}, \hat{y}) &= \hat{x}(1 - \hat{x})(1 - \hat{y}), \\ \hat{\psi}_2(\hat{x}, \hat{y}) &= \hat{x}(1 - \hat{y})\hat{y}, \\ \hat{\psi}_3(\hat{x}, \hat{y}) &= \hat{x}(1 - \hat{x})\hat{y}, \\ \hat{\psi}_4(\hat{x}, \hat{y}) &= (1 - \hat{x})(1 - \hat{y})\hat{y}, \end{aligned} \tag{24}$$

and accordingly four vector-valued edge-based bubble functions on E:

$$\boldsymbol{\psi}_i(x, y) = \mathbf{n}_i\, \psi_i(x, y) = \mathbf{n}_i\, \hat{\psi}_i(\hat{x}, \hat{y}), \quad i = 1, 2, 3, 4. \tag{25}$$

The classical Lagrangian space $Q_1(E)^2$ is now enriched as

$$\mathrm{EQ}_1(E) = Q_1(E)^2 + \mathrm{Span}(\boldsymbol{\psi}_1, \boldsymbol{\psi}_2, \boldsymbol{\psi}_3, \boldsymbol{\psi}_4). \tag{26}$$

Let Ω be a polygonal domain equipped with a shape-regular convex quadrilateral mesh $\mathcal{E}_h$. Let $\mathbf{V}_h$ be the space spanned by the previously discussed basis functions. Let $\mathbf{V}_h^0$ be the subspace of $\mathbf{V}_h$ consisting of those shape functions that vanish on $\Gamma_D^{\mathcal{E}}$. For $\mathbf{v} \in \mathbf{V}_h$, it is known that $\nabla \cdot \mathbf{v}$ is not a constant on each element E. We shall consider its average $\overline{\nabla \cdot \mathbf{v}}$ on E. This technique was known as *reduced integration* in the literature [32,36].

For the elasticity boundary value problem (18), we now establish a finite element scheme in the strain–div formulation as follows. Find $\mathbf{u}_h \in \mathbf{V}_h$ such that $\mathbf{u}_h|_{\Gamma_D^{\mathcal{E}}} = \mathbf{P}_h \mathbf{u}_D$ and

$$\mathcal{A}_h(\mathbf{u}_h, \mathbf{v}) = \mathcal{F}_h(\mathbf{v}), \qquad \forall \mathbf{v} \in \mathbf{V}_h^0, \tag{27}$$

where

$$\mathcal{A}_h(\mathbf{u}_h, \mathbf{v}) = 2\mu \sum_{E \in \mathcal{E}_h} (\varepsilon(\mathbf{u}_h), \varepsilon(\mathbf{v}))_E + \lambda \sum_{E \in \mathcal{E}_h} (\overline{\nabla \cdot \mathbf{u}_h}, \overline{\nabla \cdot \mathbf{v}})_E, \tag{28}$$

$$\mathcal{F}_h(\mathbf{v}) = \sum_{E \in \mathcal{E}_h} (\mathbf{f}, \mathbf{v})_E + \sum_{e \in \Gamma_N^{\mathcal{E}}} \langle \mathbf{t}_N, \mathbf{v} \rangle_e, \tag{29}$$

and

$$(\mathbf{P}_h \mathbf{u}_D)|_e = \tilde{\mathbf{P}}_h \mathbf{u}_D + \left(\int_e (\mathbf{u}_D - \tilde{\mathbf{P}}_h \mathbf{u}_D) \cdot \mathbf{n} \Big/ \int_e \boldsymbol{\psi}_e \cdot \mathbf{n} \right) \boldsymbol{\psi}_e, \quad e \in \Gamma_D^{\mathcal{E}}, \tag{30}$$

with $\tilde{\mathbf{P}}_h$ being the interpolation operator into $Q_1(e)^2$.

More details on the analysis and implementation of this new solver for linear elasticity can be found in [25].

4. A 2-field FE solver for poroelasticity on quadrilateral meshes

In this section, we first discuss the variational formulation for the linear poroelasticity problem (1)–(4). Then we employ the finite elements discussed in Sections 2 and 3 to develop a 2-field FE solver for the poroelasticity problem.

Let $\mathbf{V} = \mathbf{H}^1(\Omega)$ and

$$\mathbf{V}^0_{\Gamma_D^{\mathcal{E}}} = \{\mathbf{v} \in \mathbf{V} : \mathbf{v}|_{\Gamma_D^{\mathcal{E}}} = \mathbf{0}\}. \tag{31}$$

Similarly, let $V = H^1(\Omega)$ and

$$V^0_{\Gamma_D^{\mathcal{P}}} = \{q \in V : q|_{\Gamma_D^{\mathcal{P}}} = 0\}. \tag{32}$$

The variational form for the linear poroelasticity problem (1)–(4) reads as: Seek $\mathbf{u}(\cdot, t) \in \mathbf{V}$, $p(\cdot, t) \in V$ such that $\mathbf{u}(\cdot, t)|_{\Gamma_D^{\mathcal{E}}} = \mathbf{u}_D$, $p(\cdot, t)|_{\Gamma_D^{\mathcal{P}}} = p_D$ for any $t \in (0, T]$, and for $\forall \mathbf{v} \in \mathbf{V}^0_{\Gamma_D^{\mathcal{E}}}$ and $\forall q \in V^0_{\Gamma_D^{\mathcal{P}}}$, there holds

$$\begin{cases} 2\mu(\varepsilon(\mathbf{u}), \varepsilon(\mathbf{v})) + \lambda(\nabla \cdot \mathbf{u}, \nabla \cdot \mathbf{v}) - \alpha(p, \nabla \cdot \mathbf{v}) = (\mathbf{f}, \mathbf{v}) + \langle \mathbf{t}_N, \mathbf{v} \rangle_{\Gamma_N^{\mathcal{E}}}, \\ \partial_t(\alpha \nabla \cdot \mathbf{u} + c_0 p, q) + (\mathbf{K} \nabla p, \nabla q) = (s, q) - \langle u_N, q \rangle_{\Gamma_N^{\mathcal{P}}}. \end{cases} \tag{33}$$

Assume the domain Ω is equipped with a quasi-uniform convex quadrilateral mesh $\mathcal{E}_h$. Let N_t be a positive integer and $0 = t_0 < t_1 < \cdots < t_{n-1} < t_n < \cdots < t_{N_t} = T$ be a partition of the time period $[0, T]$. Denote $\Delta t_n = t_n - t_{n-1}$ for $n = 1, \ldots, N_t$.

Recall the finite element spaces $\mathbf{V}_h, \mathbf{V}_h^0$ (of vector-valued functions) discussed in Section 3. Recall also the finite element spaces S_h, S_h^0 (of scalar-valued functions) discussed in Section 2.

For $0 \leq n \leq N_t$, let $\mathbf{u}_h^{(n)} \in \mathbf{V}_h$ and $p_h^{(n)} \in S_h$ be the finite element approximations at time t_n to solid displacement and fluid pressure, respectively. Applying the implicit Euler discretization, we establish a time-marching scheme. For the initial step $n = 0$, we have

$$\mathbf{u}_h^{(0)} = \mathbf{P}_h \mathbf{u}_0, \qquad p_h^{(0)} = Q_h p_0. \tag{34}$$

For $n \geq 1$, the solid and fluid Dirichlet boundary conditions are enforced as

$$\mathbf{u}_h^{(n)}|_{\Gamma_D^{\mathcal{E}}} = \mathbf{P}_h \mathbf{u}_D, \qquad p_h^{(n,\partial)}|_{\Gamma_D^{\mathcal{D}}} = Q_h^{\partial}(p_D). \tag{35}$$

The time-marching scheme reads as

$$\begin{cases} \mathcal{A}_h^{\mathcal{E}}(\mathbf{u}_h^{(n)}, \mathbf{v}) \; - \; \mathcal{B}_h(p_h^{(n)}, \mathbf{v}) \;\; = \mathcal{F}_h^{\mathcal{E}}(\mathbf{v}), \\ \mathcal{B}_h(\mathbf{u}_h^{(n)}, q) \; + \; \mathcal{A}_h^{\mathcal{D}}(p_h^{(n)}, q) \; = \; \mathcal{F}_h^{\mathcal{D}}(q), \end{cases} \tag{36}$$

for any $\mathbf{v} \in \mathbf{V}_h^0$ and any $q \in S_h^0$. This involves three discrete bilinear forms and two linear forms that are defined as follows. First, the bilinear forms are

$$\mathcal{A}_h^{\mathcal{E}}(\mathbf{u}_h^{(n)}, \mathbf{v}) = \sum_{E \in \mathcal{E}_h} \left(2\mu \left(\varepsilon(\mathbf{u}_h^{(n)}), \varepsilon(\mathbf{v}) \right)_E + \lambda(\overline{\nabla \cdot \mathbf{u}_h^{(n)}}, \overline{\nabla \cdot \mathbf{v}})_E \right), \tag{37}$$

$$\mathcal{A}_h^{\mathcal{D}}(p_h^{(n)}, q) = \sum_{E \in \mathcal{E}_h} c_0 \left(p_h^{(n),\circ}, q^\circ \right)_{E^\circ} + \Delta t_n \left(\mathbf{K} \nabla_w p_h^{(n)}, \nabla_w q \right)_E, \tag{38}$$

$$\mathcal{B}_h(\mathbf{u}_h^{(n)}, q) = \sum_{E \in \mathcal{E}_h} \alpha(\nabla \cdot \mathbf{u}_h^{(n)}, q^\circ)_{E^\circ}. \tag{39}$$

Then the linear forms are

$$\mathcal{F}_h^{\mathcal{E}}(\mathbf{v}) = \sum_{E \in \mathcal{E}_h} (\mathbf{f}^{(n)}, \mathbf{v})_E + \sum_{e \in \Gamma_N^{\mathcal{E}}} \langle \mathbf{t}_N, \mathbf{v} \rangle_e, \tag{40}$$

$$\begin{aligned} \mathcal{F}_h^{\mathcal{D}}(q) = & \sum_{E \in \mathcal{E}_h} \Delta t_n (s^{(n)}, q^\circ)_{E^\circ} + c_0 \left(p_h^{(n-1),\circ}, q^\circ \right)_{E^\circ} + \alpha(\nabla \cdot \mathbf{u}_h^{(n-1)}, q^\circ)_{E^\circ} \\ & - \sum_{e \in \Gamma_N^{\mathcal{D}}} \langle u_N, q^\partial \rangle_e. \end{aligned} \tag{41}$$

For any time step $t_n (n = 1, 2, \ldots, N_t)$, the above 2-field finite element scheme results in a large-size sparse non-symmetric linear system that has a unique solution.

This is also called the monolithic approach since the two main variables (solid displacement and fluid pressure) are solved in a large-size single linear system, not solved through an iterative approach as compared to other finite element methods.

In the next section, we shall show that this new finite element scheme has 1st order accuracy $\mathcal{O}(h + \Delta t)$ in solid displacement and fluid pressure as measured in appropriate norms.

5. Detailed error analysis

This section presents a complete rigorous error analysis for the finite element scheme developed in the previous section.

First, we cite the following theoretical results in [13] about the regularity of the exact solutions, which will be used in our error estimates.

Theorem 1. *Let $(\mathbf{u}, p)$ be the exact solutions of the linear poroelasticity problem (1)–(5). There holds*

$$\begin{aligned} & \sup_{t \in [0,T]} \|\mathbf{u}(t)\|_{\mathbf{H}^2} + \lambda \sup_{t \in [0,T]} \|\nabla \cdot \mathbf{u}(t)\|_{\mathbf{H}^1} \\ & \lesssim C \Bigg(\sup_{t \in [0,T]} \|\mathbf{f}(t)\|_{\mathbf{L}^2} + \sup_{t \in [0,T]} \|s(t)\|_{L^2} \\ & \quad + \|\partial_t \mathbf{f}\|_{L^2(\mathbf{H}^{-1})} + \|\partial_t s\|_{L^2(L^2)} + \|p_0\|_{H^1} \Bigg), \end{aligned} \tag{42}$$

where $C > 0$ is a constant that is independent of λ. Similar regularity results about $\partial_t \mathbf{u}$, $\partial_{tt} \mathbf{u}$ can be established when further assumptions are made about the right-hand sides of the PDEs, boundary conditions, and initial data. $\square$

$$
\begin{tikzcd}
H^1(E) \arrow[r, "\nabla"] \arrow[d, "Q_h"'] & \mathbf{L}^2(E) \arrow[d, "\mathbf{Q}_h"] \\
WG(P_0, P_0) \arrow[r, "\nabla_w"'] & AC_0(E)
\end{tikzcd}
$$

Fig. 1. Commuting diagram for WG finite elements.

For ease presentation of the error analysis, we make the following assumptions.

- $c_0 = 0$. Note that c_0 corresponds to the mass term in our WG finite element discretization for Darcy flow. It does not really affect solvability, stability, or condition numbers.
- A constant hydraulic conductivity $\mathbf{K} = \kappa\mathbf{I}$.
- Homogeneous Dirichlet boundary conditions for both fluid pressure and solid displacement.
- A uniform temporal partition with $\Delta t_n = \Delta t = T/N_t$.

5.1. Preliminaries: Operators and their properties

We shall need the following operators, assuming E is a typical convex quadrilateral element and $\mathcal{E}_h$ is the whole quadrilateral mesh.

- $\mathbf{P}_h$: The interpolation operator from $\mathbf{H}^1(\Omega)$ to the global EQ_1 space on $\mathcal{E}_h$;
- π_h: Local projection into the space of elementwise constants;
- $Q_h = \{Q_h^\circ, Q_h^\partial\}$: Local L^2-projection into WG(P_0, P_0), as previously defined;
- $\mathbf{Q}_h$: Local $\mathbf{L}^2$-projection into local AC_0 spaces, as previously defined;
- Π_h: The interpolation operator from $H(\mathrm{div}, \Omega) \cap L^{2+\varepsilon}(\Omega)^2$ to the global AC_0 space on $\mathcal{E}_h$.

Lemma 1 (*WG Commuting Identity and Diagram*)**.** *For any $p \in H^1(E)$, there holds*

$$\nabla_w(Q_h p) = \mathbf{Q}_h(\nabla p). \tag{43}$$

This is illustrated as a commuting diagram in Fig. 1. See [24] also. □

Lemma 2. *For any $\mathbf{v} \in H(div, \Omega) \cap L^{2+\varepsilon}(\Omega)^2$ and any $\phi = \{\phi^\circ, \phi^\partial\} \in S_h^0$, there holds*

$$\sum_{E\in\mathcal{E}_h} (\nabla\cdot\mathbf{v}, \phi^\circ)_{E^\circ} = -\sum_{E\in\mathcal{E}_h} (\Pi_h\mathbf{v}, \nabla_w\phi)_E + \sum_{e\in\Gamma_N^{\mathcal{D}}} \langle(\Pi_h\mathbf{v})\cdot\mathbf{n}, \phi^\partial\rangle_e. \tag{44}$$

See [24] Lemma 2. □

Lemma 3. *For any $\mathbf{v} \in \mathbf{H}^1$, there holds*

(i) Firstly,

$$\pi_h(\nabla\cdot\mathbf{P}_h\mathbf{v}) = \pi_h\nabla\cdot\mathbf{v}. \tag{45}$$

(ii) Secondly, for any $q \in W_h$,

$$(\nabla\cdot(\mathbf{v} - \mathbf{P}_h\mathbf{v}), q) = 0. \tag{46}$$

Proof. See [37] Hypothesis (H2). □

Lemma 4. *For any $\mathbf{v} \in \mathbf{H}^2$, there holds*

$$\|\mathbf{v} - \mathbf{P}_h\mathbf{v}\|_k \lesssim h^{m-k}\|\mathbf{v}\|_m, \quad 0 \le k \le 1, \ 1 \le m \le 2. \tag{47}$$

Proof. See [37] Hypothesis (H2) and Lemma II.2. □

Lemma 5. *Let $\mathbf{u}^{(n)}$ be the exact solution for displacement at time t_n and $\mathbf{v} \in \mathbf{V}_h$. Then*

$$\begin{aligned}&(\nabla \cdot \mathbf{u}^{(n)}, \nabla \cdot \mathbf{v}) - (\pi_h \nabla \cdot \mathbf{u}_h^{(n)}, \pi_h \nabla \cdot \mathbf{v}) \\ &\quad = (\nabla \cdot \mathbf{u}^{(n)} - \pi_h \nabla \cdot \mathbf{u}^{(n)}, \nabla \cdot \mathbf{v}) + (\pi_h \nabla \cdot (\mathbf{P}_h \mathbf{u}^{(n)} - \mathbf{u}_h^{(n)}), \pi_h \nabla \cdot \mathbf{v}).\end{aligned} \tag{48}$$

Proof. We shall use the common technique of inserting appropriate terms. We apply Lemma 3 and the orthogonality implied by the projection operator π_h. Note that

$$\begin{aligned}\text{LHS} &= (\nabla \cdot \mathbf{u}^{(n)}, \nabla \cdot \mathbf{v}) - (\pi_h \nabla \cdot \mathbf{u}_h^{(n)}, \pi_h \nabla \cdot \mathbf{v}) \\ &= \Big((\nabla \cdot \mathbf{u}^{(n)}, \nabla \cdot \mathbf{v}) - (\pi_h \nabla \cdot \mathbf{u}^{(n)}, \nabla \cdot \mathbf{v}) \Big) \\ &\quad + \Big((\pi_h \nabla \cdot \mathbf{u}^{(n)}, \nabla \cdot \mathbf{v}) - (\pi_h \nabla \cdot \mathbf{u}^{(n)}, \pi_h \nabla \cdot \mathbf{v}) \Big) \\ &\quad\quad + \Big((\pi_h \nabla \cdot \mathbf{u}^{(n)}, \pi_h \nabla \cdot \mathbf{v}) - (\pi_h \nabla \cdot \mathbf{u}_h^{(n)}, \pi_h \nabla \cdot \mathbf{v}) \Big).\end{aligned}$$

The above 2nd group vanishes due to the orthogonality implied by π_h. Now we have

$$\begin{aligned}\text{LHS} &= \Big((\nabla \cdot \mathbf{u}^{(n)}, \nabla \cdot \mathbf{v}) - (\pi_h \nabla \cdot \mathbf{u}^{(n)}, \nabla \cdot \mathbf{v}) \Big) \\ &\quad + \Big((\pi_h \nabla \cdot \mathbf{u}^{(n)}, \pi_h \nabla \cdot \mathbf{v}) - (\pi_h (\nabla \cdot \mathbf{P}_h \mathbf{u}_h^{(n)}), \pi_h \nabla \cdot \mathbf{v}) \Big) \\ &\quad\quad + \Big((\pi_h \nabla \cdot \mathbf{P}_h \mathbf{u}_h^{(n)}, \pi_h \nabla \cdot \mathbf{v}) - (\pi_h \nabla \cdot \mathbf{u}_h^{(n)}, \pi_h \nabla \cdot \mathbf{v}) \Big).\end{aligned}$$

Interestingly, the above 2nd group vanishes also due to Lemma 3. The desired conclusion follows. □

Lemma 6 (*Taylor Expansion*)**.** *For a vectored-valued time-dependent function* $\mathbf{u}$*, there holds*

$$\begin{aligned}\frac{\mathbf{u}^{(n)} - \mathbf{u}^{(n-1)}}{\Delta t} &= \partial_t \mathbf{u}^{(n)} + \frac{1}{\Delta t} \int_{t_{n-1}}^{t_n} (\tau - t_{n-1}) \partial_{tt} \mathbf{u}(\tau) d\tau \\ &=: \partial_t \mathbf{u}^{(n)} + \mathbf{R}(\mathbf{u}, t_n),\end{aligned} \tag{49}$$

where the remainder is also shortened as $\mathbf{R}$ *for notational convenience. This formula can be found in [13]. A similar formula can be established for the fluid pressure* p *as well.* □

5.2. Error equations

Note that the displacement error $\mathbf{u}^{(n)} - \mathbf{u}_h^{(n)}$ can be split as the interpolation error $\eta_{\mathbf{u}}^{(n)}$ and the discrete error $\xi_{\mathbf{u}}^{(n)}$ that are defined as follows

$$\eta_{\mathbf{u}}^{(n)} = \mathbf{u}^{(n)} - \mathbf{P}_h \mathbf{u}^{(n)}, \qquad \xi_{\mathbf{u}}^{(n)} = \mathbf{P}_h \mathbf{u}^{(n)} - \mathbf{u}_h^{(n)}. \tag{50}$$

Likewise, we have the following quantities for pressure and pressure gradient:

$$\begin{aligned}&\eta_p^{(n)} = p^{(n)} - Q_h p^{(n)}, &&\xi_p^{(n)} = Q_h p^{(n)} - p_h^{(n)}, \\ &\eta_p^{(n),\circ} = p^{(n)} - Q_h^\circ p^{(n)}, &&\xi_p^{(n),\circ} = Q_h^\circ p^{(n)} - p_h^{(n),\circ}, \\ &\eta_{\nabla p}^{(n)} = \nabla p^{(n)} - \mathbf{Q}_h(\nabla p^{(n)}), &&\xi_{\nabla p}^{(n)} = \mathbf{Q}_h(\nabla p^{(n)}) - \nabla_w p_h^{(n)}.\end{aligned} \tag{51}$$

Note that the commuting identity in Lemma 1 implies

$$\xi_{\nabla p}^{(n)} = \nabla_w \xi_p^{(n)}. \tag{52}$$

It is obvious that

$$\begin{aligned}&\mathbf{u}^{(n)} - \mathbf{u}_h^{(n)} = \eta_{\mathbf{u}}^{(n)} + \xi_{\mathbf{u}}^{(n)}, &&p^{(n)} - p_h^{(n)} = \eta_p^{(n)} + \xi_p^{(n)}, \\ &\nabla p^{(n)} - \nabla_w p_h^{(n)} = \eta_{\nabla p}^{(n)} + \xi_{\nabla p}^{(n)}, &&p^{(n)} - p_h^{(n),\circ} = \eta_p^{(n),\circ} + \xi_p^{(n),\circ}.\end{aligned} \tag{53}$$

The main purpose of the error equations is to express the discrete errors $(\xi_{\mathbf{u}}^{(n)}, \xi_p^{(n)}, \xi_p^{(n),\circ}, \xi_{\nabla p}^{(n)})$ in terms of the interpolation errors $(\eta_{\mathbf{u}}^{(n)}, \eta_p^{(n)}, \eta_p^{(n),\circ}, \eta_{\nabla p}^{(n)})$, which are determined by regularity of the exact solutions and the approximation properties of the constructed finite element spaces.

Error Equation I. We shall first establish an error equation for displacement. Note that the finite element discretization for displacement is conforming, in other words, $\mathbf{V}_h \subset \mathbf{V}$. Thus, we have, for any $\mathbf{v} \in \mathbf{V}_h^0$,

$$2\mu \left(\varepsilon(\mathbf{u}^{(n)}), \varepsilon(\mathbf{v}) \right) + \lambda(\nabla \cdot \mathbf{u}^{(n)}, \nabla \cdot \mathbf{v}) - \alpha(p^{(n)}, \nabla \cdot \mathbf{v}) = (\mathbf{f}^{(n)}, \mathbf{v}). \tag{54}$$

The finite element scheme (the 1st equation of (36)) yields, for any $\mathbf{v} \in \mathbf{V}_h^0$,

$$2\mu(\varepsilon(\mathbf{u}_h^{(n)}), \varepsilon(\mathbf{v})) + \lambda(\pi_h \nabla \cdot \mathbf{u}_h^{(n)}, \pi_h \nabla \cdot \mathbf{v}) - \alpha(p_h^{(n),\circ}, \nabla \cdot \mathbf{v}) = (\mathbf{f}^{(n)}, \mathbf{v}). \tag{55}$$

Here, there is no need for taking the average of $\nabla\cdot\mathbf{v}$, since $p_h^{(n),\circ}$ is already a constant for the lowest order WG method.

Subtracting (55) from (54) and applying Lemma 5, we obtain

$$\begin{aligned}&2\mu\left(\varepsilon(\mathbf{u}^{(n)}-\mathbf{u}_h^{(n)}),\varepsilon(\mathbf{v})\right)\\&\quad+\lambda\Big((\nabla\cdot\mathbf{u}^{(n)}-\pi_h\nabla\cdot\mathbf{u}^{(n)},\nabla\cdot\mathbf{v})+(\pi_h\nabla\cdot(\mathbf{P}_h\mathbf{u}_h^{(n)}-\mathbf{u}_h^{(n)}),\pi_h\nabla\cdot\mathbf{v})\Big)\\&\quad-\alpha(p^{(n)}-p_h^{(n),\circ},\nabla\cdot\mathbf{v})=0.\end{aligned}$$

By the aforementioned error splitting and linearity of operators, we have

$$\begin{aligned}&2\mu\left(\varepsilon(\xi_{\mathbf{u}}^{(n)}),\varepsilon(\mathbf{v})\right)+\lambda(\pi_h\nabla\cdot\xi_{\mathbf{u}}^{(n)},\pi_h\nabla\cdot\mathbf{v})-\alpha(\xi_p^{(n),\circ},\nabla\cdot\mathbf{v})\\&\quad=-2\mu\left(\varepsilon(\eta_{\mathbf{u}}^{(n)}),\varepsilon(\mathbf{v})\right)-\lambda(\nabla\cdot\mathbf{u}^{(n)}-\pi_h\nabla\cdot\mathbf{u}^{(n)},\nabla\cdot\mathbf{v})\\&\quad+\alpha(\eta_p^{(n),\circ},\nabla\cdot\mathbf{v}),\end{aligned}\tag{56}$$

which is **the first error equation**.

Error Equation II. Now we derive the 2nd error equation. At time t_n, the 2nd PDE takes the form

$$\partial_t(\alpha\nabla\cdot\mathbf{u}^{(n)})+\nabla\cdot(-\mathbf{K}\nabla p^{(n)})=s^{(n)}.\tag{57}$$

For each element E, we apply Lemma 6 (Taylor expansion) to get, for any $q\in S_h^0$,

$$\begin{aligned}(s^{(n)},q^\circ)_{E^\circ}&=(\partial_t(\alpha\nabla\cdot\mathbf{u}^{(n)}),q^\circ)_{E^\circ}+(\nabla\cdot\left(-\mathbf{K}\nabla p^{(n)}\right),q^\circ)_{E^\circ}\\&=\alpha(\nabla\cdot\partial_t\mathbf{u}^{(n)},q^\circ)_{E^\circ}+(\nabla\cdot\left(-\mathbf{K}\nabla p^{(n)}\right),q^\circ)_{E^\circ}\\&=\alpha\left(\nabla\cdot\frac{\mathbf{u}^{(n)}-\mathbf{u}^{(n-1)}}{\Delta t},q^\circ\right)_{E^\circ}-\alpha(\nabla\cdot\mathbf{R},q^\circ)_{E^\circ}+(\nabla\cdot\left(-\mathbf{K}\nabla p^{(n)}\right),q^\circ)_{E^\circ}.\end{aligned}$$

Summing the above result over the whole mesh and applying Lemma 2 (under the assumption there is no Neumann boundary condition for pressure), we obtain

$$\begin{aligned}&\Delta t\sum_{E\in\mathcal{E}_h}(s^{(n)},q^\circ)_{E^\circ}=\alpha\sum_{E\in\mathcal{E}_h}(\nabla\cdot(\mathbf{u}^{(n)}-\mathbf{u}^{(n-1)}),q^\circ)_{E^\circ}\\&\quad-\alpha\Delta t\sum_{E\in\mathcal{E}_h}(\nabla\cdot\mathbf{R},q^\circ)_{E^\circ}+\Delta t\sum_{E\in\mathcal{E}_h}(\varPi_h(\mathbf{K}\nabla p^{(n)}),\nabla_w q)_E.\end{aligned}\tag{58}$$

Under the assumption $c_0=0$, the 2nd equation in the finite element scheme (36) can be rewritten as, for any $q\in S_h^0$,

$$\sum_{E\in\mathcal{E}_h}(s^{(n)},q^\circ)_{E^\circ}=\alpha\sum_{E\in\mathcal{E}_h}\left(\frac{\nabla\cdot\mathbf{u}_h^{(n)}-\nabla\cdot\mathbf{u}_h^{(n-1)}}{\Delta t},q^\circ\right)_{E^\circ}+\sum_{E\in\mathcal{E}_h}\left(\mathbf{K}\nabla_w p_h^{(n)},\nabla_w q\right)_E.\tag{59}$$

Combining (59), (58), and the assumption $\mathbf{K}=\kappa\mathbf{I}$, we have

$$\begin{aligned}&\alpha\sum_{E\in\mathcal{E}_h}(\nabla\cdot(\mathbf{u}^{(n)}-\mathbf{u}_h^{(n)}),q^\circ)_{E^\circ}+\Delta t\sum_{E\in\mathcal{E}_h}\kappa(\varPi_h\nabla p^{(n)}-\nabla_w p_h^{(n)},\nabla_w q)_E\\&\quad=\alpha\sum_{E\in\mathcal{E}_h}(\nabla\cdot(\mathbf{u}^{(n-1)}-\mathbf{u}_h^{(n-1)}),q^\circ)_{E^\circ}+\alpha\Delta t\sum_{E\in\mathcal{E}_h}(\nabla\cdot\mathbf{R},q^\circ)_{E^\circ}.\end{aligned}$$

We shall drop the notation for summation over the whole mesh. By splitting the errors as shown in (53), we obtain **the 2nd error equation**

$$\begin{aligned}&\alpha(\nabla\cdot(\xi_{\mathbf{u}}^{(n)}-\xi_{\mathbf{u}}^{(n-1)}),q^\circ)+\Delta t\,\kappa(\xi_{\nabla p}^{(n)},\nabla_w q)\\&\quad=-\alpha(\nabla\cdot(\eta_{\mathbf{u}}^{(n)}-\eta_{\mathbf{u}}^{(n-1)}),q^\circ)+\alpha\Delta t(\nabla\cdot\mathbf{R},q^\circ)\\&\quad-\Delta t\,\kappa(\eta_{\nabla p}^{(n)},\nabla_w q)+\Delta t\,\kappa(\nabla p^{(n)}-\varPi_h\nabla p^{(n)},\nabla_w q),\end{aligned}\tag{60}$$

where $\varPi_h\nabla p^{(n)}-\nabla_w p_h^{(n)}=\left(\varPi_h\nabla p^{(n)}-\nabla p^{(n)}\right)+\left(\nabla p^{(n)}-\nabla_w p_h^{(n)}\right)$ has been applied.

The two error equations (56) and (60) will be used in error estimation for our 2-field finite element solver.

5.3. Error estimation: Part I

Applying the elementary inequality $2ab\le a^2+b^2$, we obtain $2a(a-b)\ge a^2-b^2$, and hence two useful inequalities:

$$\begin{aligned}&2\left(\varepsilon(\xi_{\mathbf{u}}^{(n)}),\varepsilon(\xi_{\mathbf{u}}^{(n)}-\xi_{\mathbf{u}}^{(n-1)})\right)\ge\|\varepsilon(\xi_{\mathbf{u}}^{(n)})\|^2-\|\varepsilon(\xi_{\mathbf{u}}^{(n-1)})\|^2,\\&2\left(\pi_h\nabla\cdot\xi_{\mathbf{u}}^{(n)},\ \pi_h\nabla\cdot(\xi_{\mathbf{u}}^{(n)}-\xi_{\mathbf{u}}^{(n-1)})\right)\ge\|\pi_h\nabla\cdot\xi_{\mathbf{u}}^{(n)}\|^2-\|\pi_h\nabla\cdot\xi_{\mathbf{u}}^{(n-1)}\|^2.\end{aligned}\tag{61}$$

In the first error equation (56), we take $\mathbf{v} = \xi_{\mathbf{u}}^{(n)} - \xi_{\mathbf{u}}^{(n-1)}$ to obtain

$$\begin{aligned} &2\mu(\varepsilon(\xi_{\mathbf{u}}^{(n)}), \varepsilon(\xi_{\mathbf{u}}^{(n)} - \xi_{\mathbf{u}}^{(n-1)})) + \lambda\Big(\pi_h\nabla\cdot\xi_{\mathbf{u}}^{(n)},\ \pi_h\nabla\cdot(\xi_{\mathbf{u}}^{(n)} - \xi_{\mathbf{u}}^{(n-1)})\Big) \\ &\quad -\alpha(\xi_p^{(n),\circ}, \nabla\cdot(\xi_{\mathbf{u}}^{(n)} - \xi_{\mathbf{u}}^{(n-1)})) \\ &= -2\mu(\varepsilon(\eta_{\mathbf{u}}^{(n)}), \varepsilon(\xi_{\mathbf{u}}^{(n)} - \xi_{\mathbf{u}}^{(n-1)})) - \lambda(\nabla\cdot\mathbf{u}^{(n)} - \pi_h\nabla\cdot\mathbf{u}^{(n)},\ \nabla\cdot(\xi_{\mathbf{u}}^{(n)} - \xi_{\mathbf{u}}^{(n-1)})) \\ &\quad +\alpha(\eta_p^{(n),\circ}, \nabla\cdot(\xi_{\mathbf{u}}^{(n)} - \xi_{\mathbf{u}}^{(n-1)})). \end{aligned} \tag{62}$$

For the first two terms on LHS, applying (61) leads to

$$\begin{aligned} &\mu\Big(\|\varepsilon(\xi_{\mathbf{u}}^{(n)})\|^2 - \|\varepsilon(\xi_{\mathbf{u}}^{(n-1)})\|^2\Big) + \frac{\lambda}{2}\Big(\|\pi_h\nabla\cdot\xi_{\mathbf{u}}^{(n)}\|^2 - \|\pi_h\nabla\cdot\xi_{\mathbf{u}}^{(n-1)}\|^2\Big) \\ &\quad -\alpha\left(\xi_p^{(n),\circ}, \nabla\cdot(\xi_{\mathbf{u}}^{(n)} - \xi_{\mathbf{u}}^{(n-1)})\right) \\ &\le -2\mu(\varepsilon(\eta_{\mathbf{u}}^{(n)}), \varepsilon(\xi_{\mathbf{u}}^{(n)} - \xi_{\mathbf{u}}^{(n-1)})) - \lambda\Big(\nabla\cdot\mathbf{u}^{(n)} - \pi_h\nabla\cdot\mathbf{u}^{(n)},\ \nabla\cdot(\xi_{\mathbf{u}}^{(n)} - \xi_{\mathbf{u}}^{(n-1)})\Big) \\ &\quad +\alpha\left(\eta_p^{(n),\circ}, \nabla\cdot(\xi_{\mathbf{u}}^{(n)} - \xi_{\mathbf{u}}^{(n-1)})\right). \end{aligned} \tag{63}$$

In the 2nd error equation (60), we take $q = \xi_p^{(n)}$ (and hence $q^\circ = \xi_p^{(n),\circ}$) to get

$$\begin{aligned} &\alpha(\nabla\cdot(\xi_{\mathbf{u}}^{(n)} - \xi_{\mathbf{u}}^{(n-1)}), \xi_p^{(n),\circ}) + \Delta t\,\kappa(\xi_{\nabla p}^{(n)}, \nabla_w\xi_p^{(n)}) \\ &\quad = -\alpha\left(\nabla\cdot(\eta_{\mathbf{u}}^{(n)} - \eta_{\mathbf{u}}^{(n-1)}), \xi_p^{(n),\circ}\right) + \alpha\Delta t(\nabla\cdot\mathbf{R}, \xi_p^{(n),\circ}) \\ &\qquad -\Delta t\,\kappa(\eta_{\nabla p}^{(n)}, \nabla_w\xi_p^{(n)}) + \Delta t\,\kappa(\nabla p^{(n)} - \Pi_h\nabla p^{(n)}, \nabla_w\xi_p^{(n)}). \end{aligned} \tag{64}$$

By Lemma 3(ii) and the definition in (50), we have

$$(\nabla\cdot(\eta_{\mathbf{u}}^{(n)} - \eta_{\mathbf{u}}^{(n-1)}), \xi_p^{(n),\circ}) = 0.$$

We add (63) and (64) together to obtain a combined estimate

$$\begin{aligned} &\mu(\|\varepsilon(\xi_{\mathbf{u}}^{(n)})\|^2 - \|\varepsilon(\xi_{\mathbf{u}}^{(n-1)})\|^2) + \frac{\lambda}{2}\Big(\|\pi_h\nabla\cdot\xi_{\mathbf{u}}^{(n)}\|^2 - \|\pi_h\nabla\cdot\xi_{\mathbf{u}}^{(n-1)}\|^2\Big) \\ &\quad +\Delta t\,\kappa(\xi_{\nabla p}^{(n)}, \nabla_w\xi_p^{(n)}) \\ &\le -2\mu(\varepsilon(\eta_{\mathbf{u}}^{(n)}), \varepsilon(\xi_{\mathbf{u}}^{(n)} - \xi_{\mathbf{u}}^{(n-1)})) \\ &\quad -\lambda\Big(\nabla\cdot\mathbf{u}^{(n)} - \pi_h\nabla\cdot\mathbf{u}^{(n)},\ \nabla\cdot(\xi_{\mathbf{u}}^{(n)} - \xi_{\mathbf{u}}^{(n-1)})\Big) \\ &\quad +\alpha\left(\eta_p^{(n),\circ}, \nabla\cdot(\xi_{\mathbf{u}}^{(n)} - \xi_{\mathbf{u}}^{(n-1)})\right) + \alpha\Delta t(\nabla\cdot\mathbf{R}, \xi_p^{(n),\circ}) \\ &\quad -\Delta t\,\kappa(\eta_{\nabla p}^{(n)}, \nabla_w\xi_p^{(n)}) + \Delta t\,\kappa\left(\nabla p^{(n)} - \Pi_h\nabla p^{(n)}, \nabla_w\xi_p^{(n)}\right). \end{aligned} \tag{65}$$

For the above combined estimate, we shall sum from 1 to N and use the fact that $\xi_{\mathbf{u}}^{(0)} = \mathbf{0}$. Many terms will be canceled. Furthermore, we use the Korn's inequality to get

$$\mu\|\varepsilon(\xi_{\mathbf{u}}^{(N)})\|^2 \ge K_{\mathrm{Korn}}\|\xi_{\mathbf{u}}^{(N)}\|_1^2. \tag{66}$$

Finally, after applying the identity (52), we arrive at

$$\begin{aligned} &K_{\mathrm{Korn}}\|\xi_{\mathbf{u}}^{(N)}\|_1^2 + \Delta t\sum_{n=1}^{N}\kappa\|\xi_{\nabla p}^{(n)}\|^2 \\ &\le -2\mu\sum_{n=1}^{N}\left(\varepsilon(\eta_{\mathbf{u}}^{(n)}), \varepsilon(\xi_{\mathbf{u}}^{(n)} - \xi_{\mathbf{u}}^{(n-1)})\right) \\ &\quad -\lambda\sum_{n=1}^{N}\left(\nabla\cdot\mathbf{u}^{(n)} - \pi_h(\nabla\cdot\mathbf{u}^{(n)}), \nabla\cdot(\xi_{\mathbf{u}}^{(n)} - \xi_{\mathbf{u}}^{(n-1)})\right) \\ &\quad +\alpha\sum_{n=1}^{N}\left(\eta_p^{(n),\circ}, \nabla\cdot(\xi_{\mathbf{u}}^{(n)} - \xi_{\mathbf{u}}^{(n-1)})\right) + \alpha\Delta t\sum_{n=1}^{N}(\nabla\cdot\mathbf{R}, \xi_p^{(n),\circ}) \\ &\quad -\Delta t\sum_{n=1}^{N}\kappa(\eta_{\nabla p}^{(n)}, \nabla_w\xi_p^{(n)}) + \Delta t\sum_{n=1}^{N}\kappa\left(\nabla p^{(n)} - \Pi_h\nabla p^{(n)}, \nabla_w\xi_p^{(n)}\right) \\ &=: \sum_{i=1}^{6}T_i. \end{aligned} \tag{67}$$

It is interesting to notice that T_1 involves solid strain, T_2 involves solid dilation, T_3, T_4 deal with solid–fluid interaction, and T_5, T_6 are about fluid pressure gradient.

5.4. Error estimation: Part II

This part provides individual estimates for the six terms in (67). We shall frequently use the following two elementary inequalities:

- Cauchy–Schwarz inequality: $ab \lesssim a^2 + b^2$,
- A more general Young's inequality (with $\delta > 0$): $ab \lesssim \delta a^2 + \delta^{-1} b^2$.

Here we have used the notation $a \lesssim b$ for the inequality $a \le cb$ with $c > 0$ being a positive constant that is independent of the mesh size h, time step size Δt, the Lamé constant λ. But it may depend on μ, κ, α.

We shall also frequently use the technique of summation by parts:

$$\sum_{n=1}^{N} a_n(b_n - b_{n-1}) = a_N b_N - a_0 b_0 - \sum_{n=1}^{N}(a_n - a_{n-1})b_{n-1}. \tag{68}$$

Estimation on T_1. Note that μ can be absorbed into the absolute constants and we write

$$T_1 = \sum_{n=1}^{N} \left(\varepsilon(\eta_{\mathbf{u}}^{(n)}), \varepsilon(\xi_{\mathbf{u}}^{(n)} - \xi_{\mathbf{u}}^{(n-1)})\right). \tag{69}$$

Clearly, $\xi_{\mathbf{u}}^{0} = \mathbf{0}$. We apply summation by parts and Taylor expansion to obtain

$$\begin{aligned}
T_1 &= \left(\varepsilon(\eta_{\mathbf{u}}^{(N)}), \varepsilon(\xi_{\mathbf{u}}^{(N)})\right) - \sum_{n=1}^{N} \left(\varepsilon(\eta_{\mathbf{u}}^{(n)} - \eta_{\mathbf{u}}^{(n-1)}), \varepsilon(\xi_{\mathbf{u}}^{(n-1)})\right) \\
&= \left(\varepsilon(\eta_{\mathbf{u}}^{(N)}), \varepsilon(\xi_{\mathbf{u}}^{(N)})\right) - \sum_{n=1}^{N} \left(\varepsilon(\Delta t \eta_{\mathbf{u}_t}^{(n)} + \int_{t_{n-1}}^{t_n} (\tau - t_{n-1}) \eta_{\mathbf{u}_{tt}} d\tau), \varepsilon(\xi_{\mathbf{u}}^{(n-1)})\right) \\
&= \left(\varepsilon(\eta_{\mathbf{u}}^{(N)}), \varepsilon(\xi_{\mathbf{u}}^{(N)})\right) - \sum_{n=1}^{N} \Delta t \left(\varepsilon(\eta_{\mathbf{u}_t}^{(n)}), \varepsilon(\xi_{\mathbf{u}}^{(n-1)})\right) \\
&\quad - \sum_{n=1}^{N} \left(\int_{t_{n-1}}^{t_n} (\tau - t_{n-1}) \varepsilon(\eta_{\mathbf{u}_{tt}}) d\tau, \varepsilon(\xi_{\mathbf{u}}^{(n-1)})\right) \\
&=: S_1^{(1)} + S_2^{(1)} + S_3^{(1)}.
\end{aligned}$$

By Young's inequality, we have

$$\begin{aligned}
S_1^{(1)} &= \left(\varepsilon(\eta_{\mathbf{u}}^{(N)}), \varepsilon(\xi_{\mathbf{u}}^{(N)})\right) \lesssim \delta_1 \|\varepsilon(\xi_{\mathbf{u}}^{(N)})\|^2 + \delta_1^{-1} \|\varepsilon(\eta_{\mathbf{u}}^{(N)})\|^2 \\
&\lesssim \delta_1 \|\xi_{\mathbf{u}}^{(N)}\|_1^2 + \delta_1^{-1} \|\eta_{\mathbf{u}}^{(N)}\|_1^2.
\end{aligned}$$

By Cauchy–Schwarz inequality, we have

$$\begin{aligned}
S_2^{(1)} &= \Delta t \sum_{n=1}^{N} \left(\varepsilon(\eta_{\mathbf{u}_t}^{(n)}), \varepsilon(\xi_{\mathbf{u}}^{(n-1)})\right) \lesssim \Delta t \sum_{n=1}^{N} (\|\varepsilon(\eta_{\mathbf{u}_t}^{(n)})\|^2 + \|\varepsilon(\xi_{\mathbf{u}}^{(n-1)})\|^2) \\
&\lesssim \Delta t \sum_{n=0}^{N} (\|\eta_{\mathbf{u}_t}^{(n)}\|_1^2 + \|\xi_{\mathbf{u}}^{n}\|_1^2)
\end{aligned}$$

and

$$\begin{aligned}
S_3^{(1)} &= \sum_{n=1}^{N} \left(\int_{t^{(n-1)}}^{t_n} (\tau - t^{(n-1)}) \varepsilon(\eta_{\mathbf{u}_{tt}}) d\tau,\ \varepsilon(\xi_{\mathbf{u}}^{(n-1)})\right) \\
&\lesssim \sum_{n=1}^{N} \left((\Delta t)^2 \int_{t^{(n-1)}}^{t_n} \|\varepsilon(\eta_{\mathbf{u}_{tt}})\|^2 d\tau + \Delta t \|\varepsilon(\xi_{\mathbf{u}}^{(n-1)})\|^2\right) \\
&\lesssim (\Delta t)^2 \int_0^T \|\eta_{\mathbf{u}_{tt}}\|_1^2 d\tau + \Delta t \sum_{n=0}^{N} \|\xi_{\mathbf{u}}^{n}\|_1^2.
\end{aligned}$$

Combine the estimates for $S_1^{(1)}, S_2^{(1)}, S_3^{(1)}$, we obtain

$$\begin{aligned} T_1 &\lesssim \delta_1 \|\xi_{\mathbf{u}}^{(N)}\|_1^2 + \delta_1^{-1} \|\eta_{\mathbf{u}}^{(N)}\|_1^2 \\ &+ \Delta t \sum_{n=0}^{N} (\|\xi_{\mathbf{u}}^{(n)}\|_1^2 + \|\eta_{\mathbf{u}_t}^{(n)}\|_1^2) + (\Delta t)^2 \int_0^T \|\eta_{\mathbf{u}_{tt}}\|_1^2 d\tau. \end{aligned} \tag{70}$$

Estimation on T_2. We do need to keep λ in T_2 but rewrite it as

$$T_2 = \lambda \sum_{n=1}^{N} \left(\nabla \cdot \mathbf{u}^{(n)} - \pi_h \nabla \cdot \mathbf{u}^{(n)}, \nabla \cdot (\xi_{\mathbf{u}}^{(n)} - \xi_{\mathbf{u}}^{(n-1)}) \right). \tag{71}$$

We use the fact $\xi_{\mathbf{u}}^{(0)} = \mathbf{0}$, summation by parts, and Lemma 6 to obtain

$$\begin{aligned} T_2 &= \lambda(\nabla \cdot \mathbf{u}^{(N)} - \pi_h \nabla \cdot \mathbf{u}^{(N)},\ \nabla \cdot \xi_{\mathbf{u}}^{(N)}) \\ &\quad - \lambda \sum_{n=1}^{N} \left(\nabla \cdot (\mathbf{u}^{(n)} - \mathbf{u}^{(n-1)}) - \pi_h \nabla \cdot (\mathbf{u}^{(n)} - \mathbf{u}^{(n-1)}),\ \nabla \cdot \xi_{\mathbf{u}}^{(n-1)} \right) \\ &= \lambda(\nabla \cdot \mathbf{u}^{(N)} - \pi_h \nabla \cdot \mathbf{u}^{(N)},\ \nabla \cdot \xi_{\mathbf{u}}^{(N)}) \\ &\quad - \lambda\, \Delta t \sum_{n=1}^{N} \left(\nabla \cdot \mathbf{u}_t^{(n)} - \pi_h \nabla \cdot \mathbf{u}_t^{(n)},\ \nabla \cdot \xi_{\mathbf{u}}^{(n-1)} \right) \\ &\quad - \lambda \sum_{n=1}^{N} \left(\int_{t_{n-1}}^{t_n} (\tau - t_{n-1})(\nabla \cdot \mathbf{u}_{tt} - \pi_h \nabla \cdot \mathbf{u}_{tt}) d\tau,\ \nabla \cdot \xi_{\mathbf{u}}^{(n-1)} \right) \\ &=: S_1^{(2)} - S_2^{(2)} - S_3^{(2)}. \end{aligned}$$

For $S_1^{(2)}$, we apply Young's inequality and approximation properties to get

$$\begin{aligned} S_1^{(2)} &= \lambda(\nabla \cdot \mathbf{u}^{(N)} - \pi_h \nabla \cdot \mathbf{u}^{(N)},\ \nabla \cdot \xi_{\mathbf{u}}^{(N)}) \\ &\lesssim \delta_2 \|\nabla \cdot \xi_{\mathbf{u}}^{(N)}\|^2 + \delta_2^{-1} \lambda^2 \|\nabla \cdot \mathbf{u}^{(N)} - \pi_h \nabla \cdot \mathbf{u}^{(N)}\|^2 \\ &\lesssim \delta_2 \|\xi_{\mathbf{u}}^{(N)}\|_1^2 + \delta_2^{-1} h^2 \lambda^2 \|\nabla \cdot \mathbf{u}^{(N)}\|_1^2. \end{aligned}$$

For $S_2^{(2)}$, the Cauchy–Schwarz inequality and approximation properties yield

$$S_2^{(2)} \lesssim \Delta t \sum_{n=1}^{N} \left(\|\xi_{\mathbf{u}}^{(n)}\|_1^2 + h^2 \lambda^2 \|\nabla \cdot \mathbf{u}_t^{(n)}\|_1^2 \right).$$

Term $S_3^{(2)}$ can be estimated similarly and one is led to

$$\begin{aligned} T_2 &\lesssim \delta_2 \|\xi_{\mathbf{u}}^{(N)}\|_1^2 + \delta_2^{-1} h^2 \lambda^2 \|\nabla \cdot \mathbf{u}^{(N)}\|_1^2 \\ &+ \Delta t \sum_{n=1}^{N} \left(\|\xi_{\mathbf{u}}^{(n)}\|_1^2 + h^2 \lambda^2 \|\nabla \cdot \mathbf{u}_t^{(n)}\|_1^2 \right) + (\Delta t)^2 h^2 \int_0^T \lambda^2 \|\nabla \cdot \mathbf{u}_{tt}\|_1^2 d\tau. \end{aligned} \tag{72}$$

Estimation on T_3. We assume $\alpha = 1$ and write

$$T_3 = \sum_{n=1}^{N} \left(\eta_p^{(n),\circ}, \nabla \cdot (\xi_{\mathbf{u}}^{(n)} - \xi_{\mathbf{u}}^{(n-1)}) \right). \tag{73}$$

Applying summation by parts and other similar techniques, we obtain

$$\begin{aligned} T_3 &\lesssim \delta_3 \|\xi_{\mathbf{u}}^{(N)}\|_1^2 + \delta_3^{-1} \|\eta_p^{(N),\circ}\|^2 \\ &+ \Delta t \sum_{n=0}^{N} \left(\|\xi_{\mathbf{u}}^{(n)}\|_1^2 + \|\eta_{p_t}^{(n)}\|^2 \right) + (\Delta t)^2 \int_0^T \|\eta_{p_{tt}}\|^2 d\tau. \end{aligned} \tag{74}$$

Estimation on T_4. Similarly, we assume $\alpha = 1$ and rewrite

$$T_4 = \Delta t \sum_{n=1}^{N} (\nabla \cdot \mathbf{R}, \xi_p^{(n),\circ}). \tag{75}$$

By Cauchy–Schwarz inequality, we have

$$\begin{aligned}\Delta t\|\nabla\cdot\mathbf{R}\| &= \left\|\int_{t_{n-1}}^{t_n}(\tau-t_{n-1})\nabla\cdot\mathbf{u}_{tt}(\tau)d\tau\right\|\\ &\le \left\|\int_{t_{n-1}}^{t_n}(\tau-t_{n-1})d\tau\right\|\left\|\int_{t_{n-1}}^{t_n}\nabla\cdot\mathbf{u}_{tt}(\tau)d\tau\right\|\\ &\le(\Delta t)^{\frac{3}{2}}\left(\int_{t_{n-1}}^{t_n}\|\nabla\cdot\mathbf{u}_{tt}(\tau)\|^2d\tau\right)^{\frac{1}{2}}.\end{aligned}$$

Then

$$\begin{aligned}T_4 &\le \sum_{n=1}^{N}(\Delta t)^{\frac{3}{2}}\left(\int_{t_{n-1}}^{t_n}\|\nabla\cdot\mathbf{u}_{tt}(\tau)\|^2d\tau\right)^{\frac{1}{2}}\|\xi_p^{(n),\circ}\|\\ &=\sum_{n=1}^{N}\Delta t\left(\int_{t_{n-1}}^{t_n}\|\nabla\cdot\mathbf{u}_{tt}(\tau)\|^2d\tau\right)^{\frac{1}{2}}(\Delta t)^{\frac{1}{2}}\|\xi_p^{(n),\circ}\|.\end{aligned}$$

Applying Young's inequality gives

$$\begin{aligned}T_4 &\le \sum_{n=1}^{N}\left(\delta_4^{-1}(\Delta t)^2\int_{t_{n-1}}^{t_n}\|\nabla\cdot\mathbf{u}_{tt}(\tau)\|^2d\tau+\delta_4\Delta t\|\xi_p^{(n),\circ}\|^2\right)\\ &\lesssim \delta_4\Delta t\sum_{n=1}^{N}\|\xi_p^{(n),\circ}\|^2+\delta_4^{-1}(\Delta t)^2\int_0^T\|\nabla\cdot\mathbf{u}_{tt}(\tau)\|^2d\tau.\end{aligned}\tag{76}$$

Estimation on T_5. We ignore the negative sign in T_5 and rewrite it as

$$T_5=\Delta t\sum_{n=1}^{N}\kappa(\eta_{\nabla p}^{(n)},\nabla_w\xi_p^{(n)}).\tag{77}$$

We apply Young's inequality with $\delta_5=\frac{1}{4}$ and the fact $\nabla_w\xi_p^{(n)}=\xi_{\nabla p}^{(n)}$ to obtain

$$\begin{aligned}T_5 &\lesssim \Delta t\sum_{n=1}^{N}\kappa(\delta_5\|\nabla_w\xi_p^{(n)}\|^2+\delta_5^{-1}\|\eta_{\nabla p}^{(n)}\|^2)\\ &\lesssim \frac{\Delta t}{4}\sum_{n=1}^{N}\kappa\|\xi_{\nabla p}^{(n)}\|^2+4\Delta t\sum_{n=1}^{N}\kappa\|\eta_{\nabla p}^{(n)}\|^2.\end{aligned}\tag{78}$$

Estimation on T_6. Recall that

$$T_6=\Delta t\sum_{n=1}^{N}\kappa\left(\nabla p^{(n)}-\Pi_h\nabla p^{(n)},\nabla_w\xi_p^{(n)}\right).\tag{79}$$

We shall apply Young's inequality with $\delta_6=\frac{1}{4}$. We apply also the approximation properties of the global interpolation operator Π_h. Recall that $\nabla_w\xi_p^{(n)}=\xi_{\nabla p}^{(n)}$. All these together lead to

$$\begin{aligned}T_6 &\lesssim \Delta t\sum_{n=1}^{N}\kappa\left(\delta_6\|\nabla_w\xi_p^{(n)}\|^2+\delta_6^{-1}\|\nabla p^{(n)}-\Pi_h\nabla p^{(n)}\|^2\right)\\ &\lesssim \frac{\Delta t}{4}\sum_{n=1}^{N}\kappa\|\nabla_w\xi_p^{(n)}\|^2+4\Delta t\sum_{n=1}^{N}\kappa\|\nabla p^{(n)}-\Pi_h\nabla p^{(n)}\|^2\\ &\lesssim \frac{\Delta t}{4}\sum_{n=1}^{N}\kappa\|\xi_{\nabla p}^{(n)}\|^2+4\Delta t\,h^2\sum_{n=1}^{N}\kappa\|\nabla p^{(n)}\|_1^2.\end{aligned}\tag{80}$$

5.5. Error estimation: Part III

Now we combine (67) and the individual estimates on $T_i (1 \le i \le 6)$ to obtain

$$\begin{aligned}
&(K_{\text{Korn}} - \delta_1 - \delta_2 - \delta_3)\, \|\xi_{\mathbf{u}}^{(N)}\|_1^2 + \frac{1}{2}\Delta t \sum_{n=1}^{N} \kappa \|\xi_{\nabla p}^{(n)}\|^2 \\
&\lesssim \delta_1^{-1} \|\eta_{\mathbf{u}}^{(N)}\|_1^2 + \delta_2^{-1} h^2 \lambda^2 \|\nabla \cdot \mathbf{u}^{(N)}\|_1^2 + \delta_3^{-1} \|\eta_p^{(N),\circ}\|^2 \\
&+ \Delta t \sum_{n=0}^{N} \left(\|\xi_{\mathbf{u}}^{(n)}\|_1^2 + \|\eta_{\mathbf{u}_t}^{(n)}\|_1^2 + h^2\lambda^2 \|\nabla \cdot \mathbf{u}_t^{(n)}\|_1^2 + \|\eta_{p_t}^{(n)}\|^2 \right) \\
&+ (\Delta t)^2 \int_0^T \left(\|\eta_{u_{tt}}\|_1^2 + h^2\lambda^2 \|\nabla \cdot \mathbf{u}_{tt}\|_1^2 + \|\eta_{p_{tt}}\|^2 \right) d\tau \\
&+ \delta_4 \Delta t \sum_{n=1}^{N} \|\xi_p^{(n),\circ}\|^2 + \delta_4^{-1} (\Delta t)^2 \int_0^T \|\nabla \cdot \mathbf{u}_{tt}(\tau)\|^2 d\tau \\
&+ 4\Delta t \sum_{n=1}^{N} \kappa \|\eta_{\nabla p}^{(n)}\|^2 + 4\Delta t\, h^2 \sum_{n=1}^{N} \kappa \|\nabla p^{(n)}\|_1^2.
\end{aligned} \tag{81}$$

We need to relate the term $\|\xi_p^{(n),\circ}\|^2$ on the RHS to the term $\|\xi_{\nabla p}^{(n)}\|$ on the LHS.

Lemma 7. *For any $1 \le n \le N$, there holds*

$$\|\xi_p^{(n),\circ}\| \lesssim \|\nabla_w \xi_p^{(n)}\| = \|\xi_{\nabla p}^{(n)}\|. \tag{82}$$

Proof. Since $\xi_p^{(n),\circ} \in L^2(\Omega)$, by [31] Lemma 11.2.3 via solving a Poisson equation, there exists $\mathbf{w} \in \mathbf{H}^1(\Omega)$ such that

$$\nabla \cdot \mathbf{w} = \xi_p^{(n),\circ}, \qquad \|\mathbf{w}\|_{\mathbf{H}^1(\Omega)} \lesssim \|\xi_p^{(n),\circ}\|.$$

We shall use the interpolant $\Pi_h \mathbf{w}$ from the global space $\mathcal{AC}_0(\mathcal{E}_h)$, Gauss divergence theorem, definition of the discrete weak gradient, and also the fact that $\xi_p^{(n),\partial} = 0$ on $\partial\Omega$. All these together yield (first element-wise and then mesh-wise)

$$\begin{aligned}
\|\xi_p^{(n),\circ}\|^2 &= (\xi_p^{(n),\circ}, \xi_p^{(n),\circ}) = (\xi_p^{(n),\circ}, \nabla \cdot \mathbf{w}) = (\xi_p^{(n),\circ}, \nabla \cdot \Pi_h \mathbf{w}) \\
&= \langle \xi_p^{n,\partial}, (\Pi_h \mathbf{w}) \cdot \mathbf{n} \rangle - (\nabla_w \xi_p^{(n)}, \Pi_h \mathbf{w}) = -(\nabla_w \xi_p^{(n)}, \Pi_h \mathbf{w}) \\
&\le \|\nabla_w \xi_p^{(n)}\| \|\Pi_h \mathbf{w}\| \le \|\nabla_w \xi_p^{(n)}\| \|\mathbf{w}\| \le \|\nabla_w \xi_p^{(n)}\| \|\mathbf{w}\|_{\mathbf{H}^1} \\
&\lesssim \|\nabla_w \xi_p^{(n)}\| \|\xi_p^{(n),\circ}\|.
\end{aligned}$$

The normal continuity and boundedness of $\Pi_h \mathbf{w}$ along with Cauchy–Schwarz inequality have also been used. A cancellation finishes the proof. □

Now we have

$$\begin{aligned}
&(K_{\text{Korn}} - \delta_1 - \delta_2 - \delta_3)\, \|\xi_{\mathbf{u}}^{(N)}\|_1^2 + \left(\frac{1}{2} - \frac{\delta_4}{\kappa} \right) \Delta t \sum_{n=1}^{N} \kappa \|\xi_{\nabla p}^{(n)}\|^2 \\
&\lesssim \delta_1^{-1} \|\eta_{\mathbf{u}}^{(N)}\|_1^2 + \delta_2^{-1} h^2 \lambda^2 \|\nabla \cdot \mathbf{u}^{(N)}\|_1^2 + \delta_3^{-1} \|\eta_p^{(N),\circ}\|^2 + \Delta t \sum_{n=1}^{N} \|\xi_{\mathbf{u}}^{(n)}\|_1^2 \\
&+ \Delta t \sum_{n=0}^{N} \left(\|\eta_{\mathbf{u}_t}^{(n)}\|_1^2 + h^2\lambda^2 \|\nabla \cdot \mathbf{u}_t^{(n)}\|_1^2 + \|\eta_{p_t}^{(n)}\|^2 + 4\kappa \|\eta_{\nabla p}^{(n)}\|^2 + 4h^2 \kappa \|\nabla p^{(n)}\|_1^2 \right) \\
&+ (\Delta t)^2 \int_0^T \left(\|\eta_{\mathbf{u}_{tt}}\|_1^2 + h^2\lambda^2 \|\nabla \cdot \mathbf{u}_{tt}\|_1^2 + \|\eta_{p_{tt}}\|^2 + \delta_4^{-1} \|\nabla \cdot \mathbf{u}_{tt}\|^2 \right) d\tau.
\end{aligned}$$

We denote

$$\begin{aligned}
A_N &= \delta_1^{-1} \|\eta_{\mathbf{u}}^{(N)}\|_1^2 + \delta_2^{-1} h^2 \lambda^2 \|\nabla \cdot \mathbf{u}^{(N)}\|_1^2 + \delta_3^{-1} \|\eta_p^{(N),\circ}\|^2, \\
g_n &= \|\eta_{\mathbf{u}_t}^{(n)}\|_1^2 + h^2\lambda^2 \|\nabla \cdot \mathbf{u}_t^{(n)}\|_1^2 + \|\eta_{p_t}^{(n)}\|^2 + 4\kappa \|\eta_{\nabla p}^{(n)}\|^2 + 4h^2 \kappa \|\nabla p^{(n)}\|_1^2, \\
A_2 &= (\Delta t)^2 \int_0^T \left(\|\eta_{\mathbf{u}_{tt}}\|_1^2 + \|\nabla \cdot \mathbf{u}_{tt}\|^2 + h^2\lambda^2 \|\nabla \cdot \mathbf{u}_{tt}\|_1^2 + \|\eta_{p_{tt}}\|^2 \right) d\tau
\end{aligned} \tag{83}$$

and choose $\delta_1, \delta_2, \delta_3$ small enough to ensure $K_{\text{Korn}} - \delta_1 - \delta_2 - \delta_3 > 0$. We also choose δ_4 appropriately to ensure $(1/2 - \delta_4/\kappa) > 0$. Then we have

$$\|\xi_{\mathbf{u}}^{(N)}\|_1^2 + \Delta t \sum_{n=1}^{N} \kappa \|\xi_{\nabla p}^{(n)}\|^2 \lesssim \Delta t \sum_{n=1}^{N} \|\xi_{\mathbf{u}}^{(n)}\|_1^2 + \Delta t \sum_{n=0}^{N} g_n + A_2 + A_N. \tag{84}$$

By approximation properties and regularity of the exact solutions, we have

$$g_n \lesssim h^2, \qquad A_2 \lesssim (\Delta t)^2, \qquad A_N \lesssim h^2. \tag{85}$$

Applying Lemma 8 listed below, we obtain, for any $N \le N_t$,

$$\|\xi_{\mathbf{u}}^{(N)}\|_1^2 + \Delta t \sum_{n=1}^{N} \kappa \|\xi_{\nabla p}^{(n)}\|^2 \lesssim h^2 + (\Delta t)^2. \tag{86}$$

Lemma 8 (*A Discrete Gronwall Inequality*). *Let a_n, b_n, f_n, g_n be nonnegative sequences for $n = 0, 1, \ldots, N$. Let τ, B be nonnegative also such that*

$$a_N + \tau \sum_{n=0}^{N} b_n \le \tau \sum_{n=0}^{N} f_n a_n + \tau \sum_{n=0}^{N} g_n + B, \qquad n = 0, 1, \ldots \tag{87}$$

Suppose $\tau f_n < 1$ for all $n \ge 0$. Then for all $n \ge 0$, there holds

$$a_N + \tau \sum_{n=0}^{N} b_n \le exp\left(\tau \sum_{n=0}^{N} \frac{f_n}{1 - \tau f_n}\right)\left(\tau \sum_{n=0}^{N} g_n + B\right). \tag{88}$$

See [38] p.369. □

Lemma 9. *Let $(\xi_{\mathbf{u}}^{(n)}, \xi_p^{(n)}, \xi_{\nabla p}^{(n)})$ be respectively the discrete errors defined in (51). There holds*

$$\max_{1 \le n \le N} \|\xi_{\mathbf{u}}^{(n)}\|_1^2 + \Delta t \sum_{n=1}^{N} \kappa \|\xi_{\nabla p}^{(n)}\|^2 \lesssim h^2 + (\Delta t)^2, \tag{89}$$

where the absolute constant contained in the notation $\lesssim$ may depend on regularity of the exact solutions, the physical parameters μ, κ, α, but not λ and the discretization parameters $h, \Delta t$. Note this is obtained by slightly rewriting the proved estimate (86). □

Corollary 1. *Let $\xi_p^{(n),\circ}$ be the discrete error defined in (51). There holds*

$$\Delta t \sum_{n=1}^{N} \|\xi_p^{(n),\circ}\|^2 \lesssim h^2 + (\Delta t)^2. \tag{90}$$

Proof. This can be derived from Lemmas 9 and 7. □

Remark 1. Note that

$$\kappa\, \xi_{\nabla p}^{(n)} = \mathbf{Q}_h(\kappa \nabla p^{(n)}) - \kappa \nabla_w p_h^{(n)}, \tag{91}$$

where $-\kappa \nabla p^{(n)}$ is the exact Darcy velocity and $-\kappa \nabla_w p_h^{(n)}$ is the numerical Darcy velocity. If we denote the exact Darcy velocity by $\mathbf{q}$ and the numerical Darcy velocity by $\mathbf{q}_h^{(n)}$, then the above formula can be rewritten as

$$\kappa\, \xi_{\nabla p}^{(n)} = \mathbf{q}_h^{(n)} - \mathbf{Q}_h(\mathbf{q}^{(n)}). \tag{92}$$

Therefore, the estimate in Lemma 9 can be rewritten as

$$\max_{1 \le n \le N} \|\mathbf{P}_h \mathbf{u}^{(n)} - \mathbf{u}_h^{(n)}\|_{\mathbf{H}^1}^2 + \Delta t \sum_{n=1}^{N} \|\mathbf{Q}_h(\mathbf{q}^{(n)}) - \mathbf{q}_h^{(n)}\|_{\mathbf{L}^2}^2 \lesssim h^2 + (\Delta t)^2. \tag{93}$$

Theorem 2. *Let $(\mathbf{u}, p)$ be the exact solutions of (1)–(5) and $\mathbf{q} = -\mathbf{K}\nabla p$ be the Darcy velocity. Let $(\mathbf{u}_h^{(n)}, p_h^{(n)})$ be the numerical solutions of the FE scheme (36) and $\mathbf{q}_h^{(n)} = \mathbf{Q}_h(-\mathbf{K}\nabla_w p_h^{(n)})$ be the numerical Darcy velocity obtained via post-processing. Then*

Table 1
Example 1: Convergence rates of the 2-field solver EQ_1 + WG($P_0, P_0; AC_0$) on rectangular meshes with $\Delta t = 0.5^*h$.

h	$\|\mathbf{u}-\mathbf{u}_h\|_{l^\infty(\mathbf{H}^1)}$	Rate	$\|p-p_h^\circ\|_{l^2(L^2)}$	Rate	$\|\mathbf{q}-\mathbf{q}_h\|_{l^2(\mathbf{L}^2)}$	Rate
2^{-2}	2.6861E−3	–	1.8885E−3	–	1.3004E−2	–
2^{-3}	1.0937E−3	1.29	9.9499E−4	0.92	6.3866E−3	1.02
2^{-4}	5.1356E−4	1.09	5.0394E−4	0.98	3.1830E−3	1.00
2^{-5}	2.5396E−4	1.01	2.5318E−4	0.99	1.5954E−3	0.99
2^{-6}	1.2660E−4	1.00	1.2685E−4	0.99	7.9963E−4	0.99

for any $N \le N_t$, there holds

$$\max_{1\le n\le N} \|\mathbf{u}-\mathbf{u}_h^{(n)}\|_{\mathbf{H}^1}^2 + \Delta t\sum_{n=1}^N \|p^{(n)}-p_h^{(n),\circ}\|_{L^2}^2 + \Delta t\sum_{n=1}^N \|\mathbf{q}^{(n)}-\mathbf{q}_h^{(n)}\|_{\mathbf{L}^2}^2 \lesssim h^2 + (\Delta t)^2. \tag{94}$$

Proof. The above combined error estimate is obtained by applying triangle inequalities and combining the error splitting in (53), approximation properties of the constructed FE spaces, Lemma 9, Corollary 1, and Remark 1. □

6. Numerical experiments

This section presents three numerical examples for testing our 2-field finite element solver that utilizes the implicit Euler for temporal discretization, the novel WG($P_0, P_0; AC_0$) elements for Darcy flow, and the enriched Lagrangian elements EQ_1 for linear elasticity.

Example 1 (*Convergence Rates*)**.** This example is adopted from [39]. We have $\Omega = (0,1)^2$, $T = \frac{1}{2}$, $\lambda = 1$, $\mu = 1$, $\mathbf{K} = \mathbf{I}$, $c_0 = 0$, and $\alpha = 1$. For convenience of reproducibility, we provide analytical expressions for displacement, pressure, Darcy velocity, and the right-hand sides of the PDEs. First, an auxiliary function is needed

$$\psi(t) = \frac{1}{64\pi^4+4\pi^2}\left(8\pi^2\sin(2\pi t) - 2\pi\cos(2\pi t) + 2\pi e^{-8\pi^2 t}\right).$$

We have the exact solution for solid displacement as

$$\mathbf{u} = \frac{\psi(t)}{8\pi^2}\begin{bmatrix} 2\pi\cos(2\pi x)\sin(2\pi y) \\ 2\pi\sin(2\pi x)\cos(2\pi y)\end{bmatrix}$$

and the fluid pressure as

$$p = \psi(t)\sin(2\pi x)\sin(2\pi y).$$

It is interesting to see displacement, dilation, and velocity are related as

$$\nabla\cdot\mathbf{u} = -p, \qquad \mathbf{q} = -(8\pi^2)\mathbf{u}.$$

Accordingly, the body force is

$$\mathbf{f} = \frac{\psi(t)}{8\pi^2}\begin{bmatrix} 16\pi^3\cos(2\pi x)\sin(2\pi y)(2\mu+\lambda) \\ 16\pi^3\sin(2\pi x)\cos(2\pi y)(2\mu+\lambda)\end{bmatrix} + \alpha\psi(t)\begin{bmatrix} 2\pi\cos(2\pi x)\sin(2\pi y) \\ 2\pi\sin(2\pi x)\cos(2\pi y)\end{bmatrix}$$

and the fluid source is

$$s = -\left(16\pi^3\cos(2\pi t) + 4\pi^2\sin(2\pi t) - 16\pi^3 e^{-8\pi^2 t}\right)\frac{\sin(2\pi x)\sin(2\pi y)}{4\pi^2+64\pi^4} + \psi(t)8\pi^2\sin(2\pi x)\sin(2\pi y).$$

The boundary conditions are as follows. For solid, the domain right-side has a traction condition, the other three sides are specified with displacement conditions; For fluid, all boundaries have Dirichlet boundary conditions.

Shown in Table 1 are results for Example 1. One observes 1st order convergence rates in displacement $\mathbf{H}^1$-norm, pressure L^2-norm, and velocity $\mathbf{L}^2$-norm.

Shown in Fig. 2 are results at the final time $T = 0.5$ with $h = 1/32$. The top panel shows fluid pressure and Darcy (seepage) velocity. The bottom panel shows elementwise solid dilation along with a deformed mesh that is determined by the nodal displacements. Since the displacement values are at the magnitude of 10^{-3}, the deformation is magnified by 200 times for better visualization. These two panels together reveal the basic physical processes in linear poroelasticity. We examine specifically the lower-left quadrant. As the solid is being compressed from the bottom and left sides, the fluid

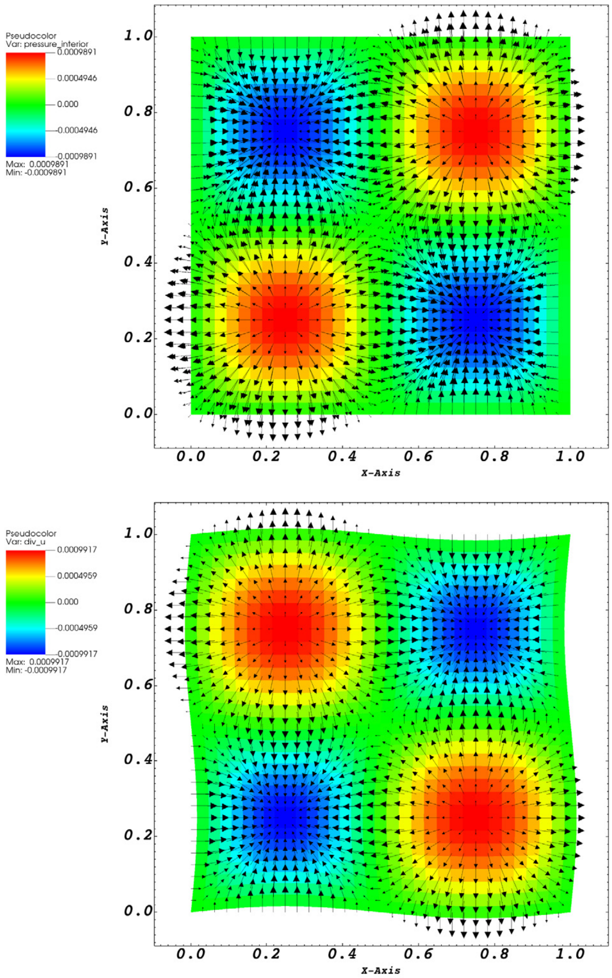

Fig. 2. Ex. 1: Numerical results at the final time $T = 0.5$ obtained on a rectangular mesh with $h = 1/32$ and $\Delta t = 0.5 * h$. *Top*: Profiles of fluid pressure and velocity; *Bottom*: Nodal displacements and elementwise dilation along with the deformed mesh (magnified by 200 times for better visual effect).

flows out from the bottom and left sides, which agrees with the pressure drop from domain interior to the peripheral. The solid is shrinking with negative dilation due to the inward displacement from the peripheral.

Example 2 (*Locking-free*)**.** This example is derived from [40,41]. Here $\Omega = (0, 1)^2$, $T = 1$, $\mu = 1$, $\mathbf{K} = \kappa\mathbf{I}$, $c_0 = 0$, and $\alpha = 1$. The fluid pressure is

$$p = \sin\left(\frac{\pi}{2}t\right)\frac{\pi}{\lambda}\sin(\pi(x+y)),$$

the solid displacement is

$$\mathbf{u} = \sin\left(\frac{\pi}{2}t\right)\left(\begin{bmatrix} \frac{\pi}{2}\sin^2(\pi x)\sin(2\pi y) \\ -\frac{\pi}{2}\sin^2(\pi y)\sin(2\pi x)\end{bmatrix} + \frac{1}{\lambda}\begin{bmatrix}\sin(\pi x)\sin(\pi y) \\ \sin(\pi x)\sin(\pi y)\end{bmatrix}\right). \tag{95}$$

It is interesting to see that

$$\nabla \cdot \mathbf{u} = p.$$

We pose Dirichlet boundary conditions on the whole boundary for both fluid and solid. A noticeable feature is that $\nabla \cdot \mathbf{u} \to 0$ as $\lambda \to \infty$. This mimics the "nearly incompressible" property of an elastic material.

In numerical experiments, we set $\kappa = 1$ but test $\lambda = 1$ and $\lambda = 10^6$. A sequence of rectangular meshes are used along with $\Delta t = h$. The results in Tables 2 and 3 demonstrate the **λ-independence** of the convergence rates for this solver.

Table 2
Example 2: Convergence rates of the 2-field solver EQ_1 + WG($P_0, P_0; AC_0$) on rectangular meshes with $\Delta t = h$ for the case $\lambda = 1$.

h	$\|\mathbf{u} - \mathbf{u}_h\|_{l^\infty(\mathbf{H}^1)}$	Rate	$\|p - p_h^\circ\|_{L^2(L^2)}$	Rate	$\|\mathbf{q} - \mathbf{q}_h\|_{L^2(\mathbf{L}^2)}$	Rate
2^{-2}	1.854E−00	–	5.504E−01	–	1.781E−00	–
2^{-3}	8.574E−01	1.11	2.656E−01	1.05	8.422E−01	1.08
2^{-4}	4.186E−01	1.03	1.296E−01	1.03	4.085E−01	1.04
2^{-5}	2.080E−01	1.00	6.392E−02	1.02	2.011E−01	1.02
2^{-6}	1.038E−01	1.00	3.172E−02	1.01	9.976E−02	1.01

Table 3
Example 2: Numerical results of the 2-field solver on rectangular meshes with $\Delta t = h$ for the case $\lambda = 10^6$.

h	$\|\mathbf{u} - \mathbf{u}_h\|_{l^\infty(\mathbf{H}^1)}$	Rate	$\|p - p_h^\circ\|_{L^2(L^2)}$	Rate	$\|\mathbf{q} - \mathbf{q}_h\|_{L^2(\mathbf{L}^2)}$	Rate
2^{-2}	1.782E−00	–	5.504E−07	–	1.782E−06	–
2^{-3}	8.193E−01	1.12	2.656E−07	1.05	8.425E−07	1.08
2^{-4}	3.991E−01	1.03	1.296E−07	1.03	4.086E−07	1.04
2^{-5}	1.982E−01	1.00	6.392E−08	1.02	2.011E−07	1.02
2^{-6}	9.894E−02	1.00	3.172E−08	1.01	9.976E−08	1.01

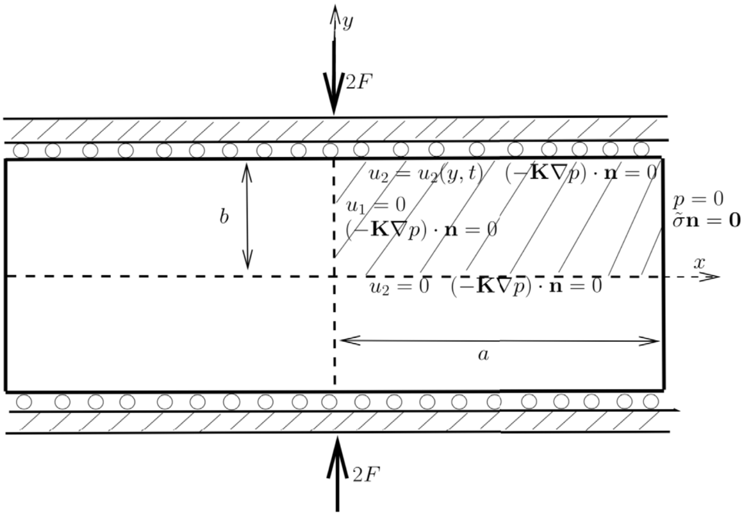

Fig. 3. Ex.3 (Mandel's problem): Illustration.

Example 3 (*Mandel's Problem*)**.** This is a frequently tested benchmark that has known analytical solutions, although the solutions are in the form of infinite series. See [8,16,21,42,43]. The problem involves a poroelastic rectangular slab with extent $2a$ in the x-direction and extent $2b$ in the y-direction being sandwiched by two rigid plates at the top and the bottom. Two forces of magnitude $2F$, pointing to the slab, are applied at the top and bottom plates, respectively. Due to the rigidity of the plates, the slab remains in contact with the two plates. This implies that the vertical displacement at the top and bottom are uniform. The initial condition for displacement is $\mathbf{u}(x, y, 0) = \mathbf{0}$. Based on symmetry in the problem, we choose the center of the slab as the origin and consider the upper-right quadrant. Mathematically, the Mandel's problem is thus posed for the domain $\Omega = (0, a) \times (0, b)$ for a certain time period $[0, T]$. See Fig. 3 for an illustration.

The boundary conditions for the solid part are

(i) Symmetry or partial Dirichlet: $u_1 = 0$ for $x = 0$; $u_2 = 0$ for $y = 0$;
(ii) Neumann or traction-free: $\tilde{\sigma}\mathbf{n} = \mathbf{0}$ for $x = a$;
(iii) Specially, for $y = b$ (the top side), it is subject to the traction condition $\tilde{\sigma}\mathbf{n} = [0, -2F]$ along with the "rigid plate" constraint, which requires u_2 stays the same for the whole top side.

The boundary conditions for the fluid part are

(iv) Dirichlet: $p = 0$ for $x = a$ (drained);
(v) Neumann or no-flow: $(-\mathbf{K}\nabla p) \cdot \mathbf{n} = 0$ for $x = 0, y = 0, y = b$.

It is non-trivial to implement condition (iii). However, we have known exact solutions for this problem. An easier but essentially equivalent treatment would be imposing a partial Dirichlet boundary condition for u_2 using the known exact solution for displacement (to be presented later), as done in [42,43].

The physical parameters in this problem are as follows.

- ν is the Poisson ratio, E is the Young's modulus, λ, μ are Láme constants;
- B is the Skempton's coefficient;
- The undrained Poisson's ratio is

$$\nu_u = \frac{3\nu + B(1-2\nu)}{3 - B(1-2\nu)}; \tag{96}$$

- The hydraulic conductivity is $\mathbf{K} = \kappa \mathbf{I}$;
- The consolidation coefficient is

$$c_f = \kappa(\lambda + 2\mu). \tag{97}$$

In addition, we have $\alpha_n > 0$ as the nth root of the nonlinear algebraic equation

$$\tan(\alpha_n) = \frac{1-\nu}{\nu_u - \nu}\,\alpha_n, \qquad n = 1, 2, \ldots \tag{98}$$

and

$$A_n = \frac{\sin(\alpha_n)}{\alpha_n - \sin(\alpha_n)\cos(\alpha_n)}, \quad B_n = \frac{\cos(\alpha_n)}{\alpha_n - \sin(\alpha_n)\cos(\alpha_n)}. \tag{99}$$

For convenience, we use these two normalized variables

$$\hat{x} = \frac{x}{a}, \quad \hat{t} = \frac{c_f}{a^2} t \tag{100}$$

in the known analytical solutions for the problem.

- The exact solution for fluid pressure is known to be independent of y:

$$\frac{p(x,y,t)}{\frac{F}{a}\frac{B(1+\nu_u)}{3}} = 2\sum_{n=1}^{\infty} A_n e^{-\alpha_n^2 \hat{t}} \left(\cos(\alpha_n \hat{x}) - \cos\alpha_n\right) =: \hat{p}(\hat{x}, \hat{t}), \tag{101}$$

  where $\hat{p}(\hat{x}, \hat{t})$ is interpreted as the normalized pressure.
- The analytical solution for solid displacement is

$$\frac{u_1}{F/a} = \left(\frac{\nu}{2\mu} - \frac{\nu_u}{\mu}\sum_{n=1}^{\infty} A_n e^{-\alpha_n \hat{t}} \cos\alpha_n\right)x + \frac{a}{\mu}\sum_{n=1}^{\infty} B_n e^{-\alpha_n^2 \hat{t}} \sin(\alpha_n \hat{x}) \tag{102}$$

  and

$$\frac{u_2}{F/a} = \left(-\frac{1-\nu}{2\mu} + \frac{1-\nu_u}{\mu}\sum_{n=1}^{\infty} A_n e^{-\alpha_n^2 \hat{t}} \cos\alpha_n\right)y. \tag{103}$$

  Note that u_1 is independent of y and u_2 is independent of x.
- For solid stress, it is known that $\sigma_{xx} = \sigma_{xy} = 0$ and

$$\frac{\sigma_{yy}}{F/a} = -1 + 2\sum_{n=1}^{\infty} A_n e^{-\alpha_n^2 \hat{t}} \left(\cos\alpha_n - \frac{B(\nu_u - \nu)}{1-\nu}\cos(\alpha_n \hat{x})\right) =: \widehat{\sigma}_{yy}. \tag{104}$$

  Similarly, $\widehat{\sigma}_{yy}$ is interpreted as the normalized effective stress.

For numerical experiments, we set $a = b = 1$, $F = 1$, $E = 10^4$, $\nu = 0$ or $\nu = 0.4$, $B = 1$, and hence $\nu_u = 0.5$. Furthermore, $\kappa = 10^{-6}$ and c_f is calculated accordingly. We have also $c_0 = 0$ and $\alpha = 1$.

We test our solver on a rectangular mesh with $h = 1/32$ with $\Delta t = 10^{-1}$.

Fig. 4 demonstrates good approximation in pressure. The left panel is for Poisson ratio $\nu = 0$ (a bit unusual though), which has been frequently tested in the literature [8,42,43]. The right panel shows pressure profiles for $\nu = 0.4$. One can see relatively faster pressure drop. As ν gets closer to the limit value 0.5, the material is closer being incompressible, which implies fast fluid drainage and hence faster pressure drop. This can also be deduced from the exact pressure expression in Eq. (101). When other parameters are fixed, larger ν implies larger roots α_n in Eq. (98) and hence faster decay of the exponential terms in Eq. (101).

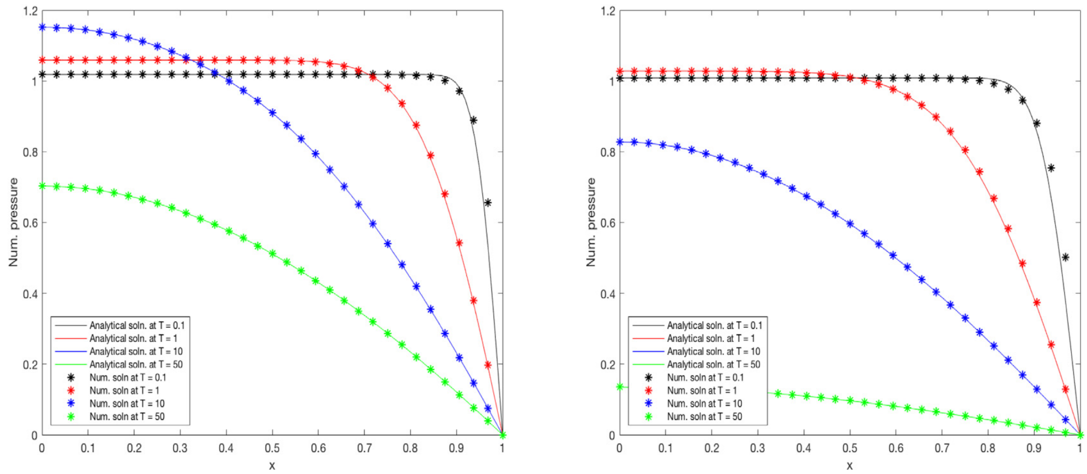

Fig. 4. Ex.3 (Mandel's problem): Pressure profiles. *Left*: $\nu = 0$; *Right*: $\nu = 0.4$.

7. Concluding remarks

In this paper, we have developed a finite element solver for linear poroelasticity aiming at reviving the 2-field approach. Darcy flow is discretized by the novel weak Galerkin $(P_0, P_0; AC_0)$ finite elements [24,30] whereas linear elasticity is discretized by the enriched Lagrangian elements (EQ_1) [25]. Both types of finite elements apply to general convex quadrilateral meshes. By coupling the elementwise averages of dilation (divergence of displacement) with the constant pressure for element interiors, the FE scheme produces stable and accurate numerical solutions that are locking-free, as validated by rigorous analysis and numerical experiments.

As demonstrated in this paper, the WG finite element methodology has some nice features.

- WG provides flexibility in construction of discrete weak gradients (or other operators) in certain spaces that have the desired approximation properties. In particular for poroelasticity studied in this paper, we choose the Arbogast-Correa spaces on quadrilaterals.
- The WG methodology holds some advantages over the classical MFEMs, since only the (elementwise) local bases are needed in the construction of discrete weak gradients. On the contrary, MFEMs need to construct a global basis for an $H(\mathrm{div})$-subspace, which is far from easy in certain cases.
- WG can be well integrated with other FEMs, e.g., the continuous Galerkin type enriched Lagrangian finite element methods (adopted for linear elasticity in this paper).

The 2-field FE solver in this paper can be extended to three dimensions. Cuboidal hexahedral meshes will be used. As 3-dim analogues of the $\mathrm{AC}_k(k \geq 0)$ spaces, the $\mathrm{AT}_k(k \geq 0)$ spaces [44] will be used. But they shall be used in the WG framework for spatial discretization of Darcy flow. The WG methodology allows use of local bases for elementwise AT_k spaces and avoid arduous construction of a global basis for the AT_k space for the whole mesh in the classical MFEM approach. An open-access implementation of such a solver is currently under our investigation and will be reported in our future work.

The FE solver developed in this paper considers a monolithic system that couples spatial discretizations of both fluid pressure and solid displacement. An alternative approach is an iterative coupling of two independent solvers for Darcy flow and linear elasticity, as investigated in [45]. This permits treatment of a stress-dependent permeability in nonlinear poroelasticity [17]. This is currently under our investigation and will be reported in our future work.

Acknowledgments

J. Liu was supported in part by US National Science Foundation under Grant DMS-1819252. S. Tavener was partially supported by US National Science Foundation under Grant DMS-1720473. Z. Wang was supported in part by Grant 74120–18841215 from Sun Yat-sen University (China).

References

[1] Joseph Haemer, Dennis Carter, Nicholas Giori, The low permeability of healthy meniscus and labrum limit articular cartilage consolidation and maintain fluid load support in the knee and hip, J. Biomech. 45 (2012) 1450–1456.

[2] Emad Moeendarbary, Léo Valon, Marco Fritzsche, Andrew Harris, Dale Moulding, Adrian Thrasher, Eleanor Stride, L. Mahadevan, Guillaume Charras, The cytoplasm of living cells behaves as a poroelastic material, Nature Mater. 12 (2013) 253–261.

[3] Karen Støverud, Melanie Darcis, Rainer Helmig, S. Majid Hassanizadeh, Modeling concentration distribution and deformation during convection-enhanced drug delivery into brain tissue, Transp. Porous Media 92 (2012) 119–143.
[4] Benjamin Wheatley, Kristine Fischenich, Keith Button, Roger Haut, Tammy Donahue, An optimized transversely isotropic, hyper-poro-viscoelastic finite element model of the meniscus to evaluate mechanical degradation following traumatic loading, J. Biomech. 48 (2015) 1454–1460.
[5] Maurice Biot, General theory of three-dimensional consolidation, J. Appl. Phys. 12 (1941) 155–164.
[6] Ralph Showalter, Diffusion in poro-elastic media, J. Math. Anal. Appl. 251 (2000) 310–340..
[7] Graham Harper, Jiangguo Liu, Simon Tavener, Zhuoran Wang, A two-field finite element solver for poroelasticity on quadrilateral meshes, Lect. Notes Comput. Sci. 10862 (2018) 76–88.
[8] Xiaozhe Hu, Lin Mu, Xiu Ye, Weak Galerkin method for the Biot's consolidation model, Comput. Math. Appl. 75 (2018) 2017–2030.
[9] Roland Lewis, Bernard Schrefler, The Finite Element Method in the Static and Dynamic Deformation and Consolidation of Porous Media, second ed., Wiley, 1999.
[10] Lorenz Berger, Rafel Bordas, David Kay, Simon Tavener, Stabilized lowest-order finite element approximation for linear three-field poroelasticity, SIAM J. Sci. Comput. 37 (2015) A2222–A2245.
[11] Xiaozhe Hu, Carmen Rodrigo, Francisco Gaspar, Ludmil Zikatanov, A nonconforming finite element method for the Biot's consolidation model in poroelasticity, J. Comput. Appl. Math. 310 (2017) 143–154.
[12] Phillip Phillips, Mary Wheeler, A coupling of mixed with discontinuous Galerkin finite element methods for poroelasticity, Comput. Geosci. 12 (2008) 417–435.
[13] Son-Young Yi, A study of two modes of locking in poroelasticity, SIAM J. Numer. Anal. 55 (2017) 1915–1936.
[14] Son-Young Yi, Convergence analysis of a new mixed finite element method for Biot's consolidation model, Numer. Methods Partial Differential Equations 30 (2014) 1189–1210.
[15] Phillip J. Phillips, Mary F. Wheeler, Overcoming the problem of locking in linear elasticity and poroelasticity: an heuristic approach, Comput. Geosci. 13 (2009) 5–12.
[16] Y. Abousleiman, A.D. Cheng, L. Cui, E. Detournay, J. Roegiers, Mandel's problem revisted, Geotechnique 46 (1996) 187–195.
[17] Silvia Barbeiro, Mary Wheeler, A priori error estimates for the numerical solution of a coupled geomechanics and reservoir flow model with stress-dependent permeability, Comput. Geosci. 14 (2010) 755–768.
[18] Martina Bukac, Ivan Yotov, R. Zakerzadeh, Paolo Zunino, Partitioning strategies for the interaction of a fluid with a poroelastic material based on a Nitsche's coupling approach, Comput. Methods Appl. Mech. Engrg. 292 (2015) 138–170.
[19] Yanzhao Cao, Song Chen, Amnon Meir, Quasilinear poroelasticity: Analysis and hybrid finite element approximation, Numer. Methods Partial Differential Equations 31 (2015) 1174–1189.
[20] Phillip Phillips, Finite Element Methods in Linear Poroelasticity: Theoretical and Computational Results (PhD thesis), University of Texas at Austin, 2005.
[21] Phillip Phillips, Mary Wheeler, A coupling of mixed with continuous Galerkin finite element methods for poroelasticity i: the continuous in time case, Comput. Geosci. 11 (2007) 131–144.
[22] Ming Sun, Hongxing Rui, A coupling of weak Galerkin and mixed finite element methods for poroelasticity, Comput. Math. Appl. 73 (2017) 804–823.
[23] Mary Wheeler, Guangri Xue, Ivan Yotov, Coupling multipoint flux mixed finite element methods with continuous Galerkin methods for poroelasticity, Comput. Geosci. 18 (2014) 57–75.
[24] Jiangguo Liu, Simon Tavener, Zhuoran Wang, Penalty-free any-order weak Galerkin FEMs for elliptic problems on quadrilateral meshes, J. Sci. Comput. 83 (2020) Article #47.
[25] Graham Harper, Ruishu Wang, Jiangguo Liu, Simon Tavener, Ran Zhang, A locking-free solver for linear elasticity on quadrilateral and hexahedral meshes based on enrichment of Lagrangian elements, Comput. Math. Appl. 80 (2020) 1578–1595.
[26] Guang Lin, Jiangguo Liu, Lin Mu, Xiu Ye, Weak Galerkin finite element methdos for Darcy flow: Anistropy and heterogeneity, J. Comput. Phys. 276 (2014) 422–437.
[27] Jiangguo Liu, Simon Tavener, Zhuoran Wang, Lowest-order weak Galerkin finite element method for Darcy flow on convex polygonal meshes, SIAM J. Sci. Comput. 40 (2018) B1229–B1252.
[28] F. Brezzi, M. Fortin, Mixed and Hybrid Finite Element Methods, Springer-Verlag, 1991.
[29] D.N. Arnold, D. Boffi, R.S. Falk, Quadrilateral H(div) finite elements, SIAM J. Numer. Anal. 42 (2005) 2429–2451.
[30] Todd Arbogast, Maicon Correa, Two families of H(div) mixed finite elements on quadrilaterals of minimal dimension, SIAM J. Numer. Anal. 54 (2016) 3332–3356.
[31] Susanne C. Brenner, L. Ridgway Scott, The mathematical theory of finite element methods, third ed., in: Texts in Applied Mathematics, vol. 15, Springer-Verlag, New York, 2008.
[32] Susanne Brenner, Li-Yeng Sung, Linear finite element methods for planar linear elasticity, Math. Comp. 59 (1992) 321–338.
[33] Jun Hu, Hongying Man, Jianye Wang, Shangyou Zhang, The simplest nonconforming mixed finite element method for linear elasticity in the symmetric formulation on n-rectangular grids, Comput. Math. Appl. 71 (2016) 1317–1336.
[34] Bishnu P. Lamichhane, A mixed finite element method for nearly incompressible elasticity and Stokes equations using primal and dual meshes with quadrilateral and hexahedral grids, J. Comput. Appl. Math. 260 (2014) 356–363..
[35] Dubravka Mijuca, On hexahedral finite element HC8/27 in elasticity, Comput. Mech. 33 (2004) 466–480.
[36] David S. Malkus, Thomas Hughes, Mixed finite element methods - reduced and selective integration techniques: A unification of concepts, Comput. Methods Appl. Mech. Engrg. 15 (1978) 63–81.
[37] Christine Bernardi, Geneviève Raugel, Analysis of some finite elements for the Stokes problem, Math. Comp. 44 (1985) 71–79.
[38] John G. Heywood, Rolf Rannacher, Finite-element approximation of the nonstationary Navier-Stokes problem Part IV: Error analysis for second-order time-discretization, SIAM J. Numer. Anal. 27 (1990) 353–384.
[39] Guido Kanschat, Beatrice Riviere, A finite element method with strong mass conservation for Biot's linear consolidation model, J. Sci. Comput. 77 (2018) 1762–1779.
[40] C. Carstensen, M. Schedensack, Medius analysis and comparison results for first-order finite element methods in linear elasticity, IMA J. Numer. Anal. 35 (2015) 1591–1621.
[41] Graham Harper, Jiangguo Liu, Simon Tavener, Bin Zheng, Lowest-order weak Galerkin finite element methods for linear elasticity on rectangular and brick meshes, J. Sci. Comput. 78 (2019) 1917–1941.
[42] Maicon R. Correa, Marcio A. Murad, A new sequential method for three-phase immiscible flow in poroelastic media, J. Comput. Phys. 373 (2018) 493–532.
[43] Carmen Rodrigo, Francisco Gaspar, Xiaozhe Hu, Ludmil Zikatanov, Stability and monotonicity for some discretizations of the Biot's consolidation model, Comput. Methods Appl. Mech. Engrg. 298 (2016) 183–204.
[44] Todd Arbogast, Zhen Tao, Construction of H(div)-conforming mixed finite elements on cuboidal hexahedra, Numer. Math. 142 (2019) 1–32.
[45] Mary Wheeler, Xiuli Gai, Iteratively coupled mixed and Galerkin finite element methods for poro-elasticity, Numer. Methods Partial Differential Equations 23 (2007) 785–797.